Greene, H.G., Collot, J.-Y., Stokking, L.B., et al., 1994
Proceedings of the Ocean Drilling Program, Scientific Results, Vol. 134

8. DIAGENESIS AND HYDROLOGY AT THE NEW HEBRIDES FOREARC AND INTRA-ARC AOBA BASIN[1]

Jonathan B. Martin[2]

ABSTRACT

Depending on the temperature and the extent of diagenetic alteration of fluid chemistry, fluid flow at convergent margins may transfer important quantities of heat and mass between the crust and seawater, thereby influencing global mass, isotopic and heat budgets. In the North Aoba Basin, an intra-arc basin located at the New Hebrides Island Arc, alteration of volcanic ash to clay minerals and zeolites forms a $CaCl_2$ brine, perhaps in less than 1 to 3 m.y. The brine results from an exchange of Ca for Na, K, and Mg, and an increase in Cl concentrations to a maximum of 1241 mM. The Cl increase is partly due to the transfer of H_2O from the pore fluid into authigenic minerals, but water mass balances, $\delta^{18}O$-Cl correlations, and Br/Cl ratios suggest that there is a source of Cl in the sediments. Concentration profiles indicate that Li is transferred from the fluid to solid phase at depths <300 meters below seafloor (mbsf), but at greater depths it is transferred from the solid to fluid phase, at temperatures possibly as low as 25°C.

In the accretionary wedge extensive fluid flow appears to be confined to highly faulted regions. Although Cl concentrations less than seawater value are common at convergent margins, the New Hebrides margin contains little low-Cl fluid. Br/Cl ratios suggest the low-Cl fluid is from dilution, and $\delta^{18}O$ values indicate the water may be derived from mineral dehydration and mixing with meteoric water. The New Hebrides margin exhibits few surface manifestations of venting (e.g., sulfide-oxidizing benthic biological communities, carbonate crusts, mud volcanoes) and thus fluid fluxes may be smaller than at many other margins.

INTRODUCTION

At convergent margins, the flow of fluids between Layers I and II of the oceanic crust and seawater could carry important fluxes of heat and mass, thereby influencing their global distributions (Han and Suess, 1989; Kastner et al., 1991; Martin et al., 1991). The origins of the fluids and the magnitudes of their fluxes are not precisely known. Some fluid flow is caused simply by porosity reduction during tectonic compaction of the accreted sediment (von Huene and Lee, 1983; Bray and Karig, 1985; Fowler et al., 1985; Carson et al., 1990); this flow is estimated to flux to the oceans at the rate of ~1 km^3 water/yr (COSOD II, 1987). At certain convergent margins, however, flow volumes are greater than those that can be sustained by porosity reduction alone, implying that some fluids originate from regions external to the margin (Le Pichon et al., 1990, 1991; Kastner et al., 1991). The magnitudes of heat and mass fluxes depend directly on the volumes, temperatures and compositions of the advecting fluids. Because temperatures generally increase with burial depth, vertical fluid advection would transport the greatest quantities of heat. The depth distributions of fluid compositions are more complex than the heat distributions and depend on the origins of the fluids, on their hydrology, and on several important fluid-solid reactions. For any particular margin, the dominating fluid-solid reactions are controlled by the types of basement rocks and sediments, while the reaction rates are controlled by the temperatures. Although a variety of sediment types is found at convergent margins, every convergent margin is a site of active volcanism, and ash is an important component of all margin sediments. The ash is diluted to various degrees by other components, commonly biogenic and terrigenous detritus. Because basaltic ash is highly unstable in the marine environment, its alteration is one of the important fluid-solid reactions altering pore-fluid chemistry, even when greatly diluted by other phases.

The tectonic setting and sedimentology of the New Hebrides convergent margin (Fig. 1; Collot et al., 1985; Greene and Wong, 1988; Collot and Fisher, 1991; Fisher et al., 1991; Collot, Greene, Stokking, et al., 1992) provide an ideal location to study fluid flow in forearc sediments and alteration of pore fluid chemistry caused by volcanic ash diagenesis. Sediments at the margin are composed mostly of volcanic ash and breccias and biogenic carbonate (Fig. 2). Collision of the d'Entrecasteaux Zone (DEZ; Daniel and Katz, 1981; Collot et al., 1985; Marthelot et al., 1985) contributes to the accretion of material from the subducting Australian Plate onto the overriding Pacific Plate and creates rapid porosity reduction within the accretionary wedge (Leonard and Ask, this volume). The collision also uplifts Espiritu Santo and Malakula islands (Taylor, 1992) thereby forming the intra-arc Aoba Basin (Fig. 1). This basin traps sediments that are rapidly deposited at rates of 100 to 300 m/m.y. (Collot, Greene, Stokking, et al., 1992). Because there is less deviatoric stress in the basin than in the accretionary wedge and only a small hydrologic head from the surrounding islands, there should be little or no lateral fluid flow through the basin sediments. Pore-fluid concentrations that deviate from seawater values therefore would result solely from fluid-solid reactions and subsequent diffusion. The dominating fluid-solid reactions thus would be reflected in the pore-fluid concentration gradients and the quantities and types of authigenic minerals. Because similar sediment types are found in the North Aoba Basin and the accretionary wedge (Fig. 2), the same diagenetic reactions would be important in both regions. In the accreted sediment, deviations from the predicted pore-fluid compositional changes based on the important diagenetic reactions could indicate horizons of fluid flow and the presence of fluids with origins external to the accretionary wedge. The chemical and isotopic compositions would reflect the origins of these externally derived fluids.

Specific problems to be addressed in this paper include documenting the important diagenetic reactions and the resulting chemical and isotopic changes in non-advecting pore fluids, determining the major authigenic phases formed during these reactions, estimating a mass balance for the exchange of water between the fluid and solid phases, and relating the reactions to the temperatures based on the observed geothermal gradients. Additional important problems, specific to the accretionary wedge pore fluids, include identifying horizons of fluid

[1] Greene, H.G., Collot, J.-Y., Stokking, L.B., et al., 1994. *Proc. ODP, Sci. Results,* 134: College Station, TX (Ocean Drilling Program).
[2] Scripps Institution of Oceanography, University of California–San Diego, La Jolla, CA 92093-0208, U.S.A.

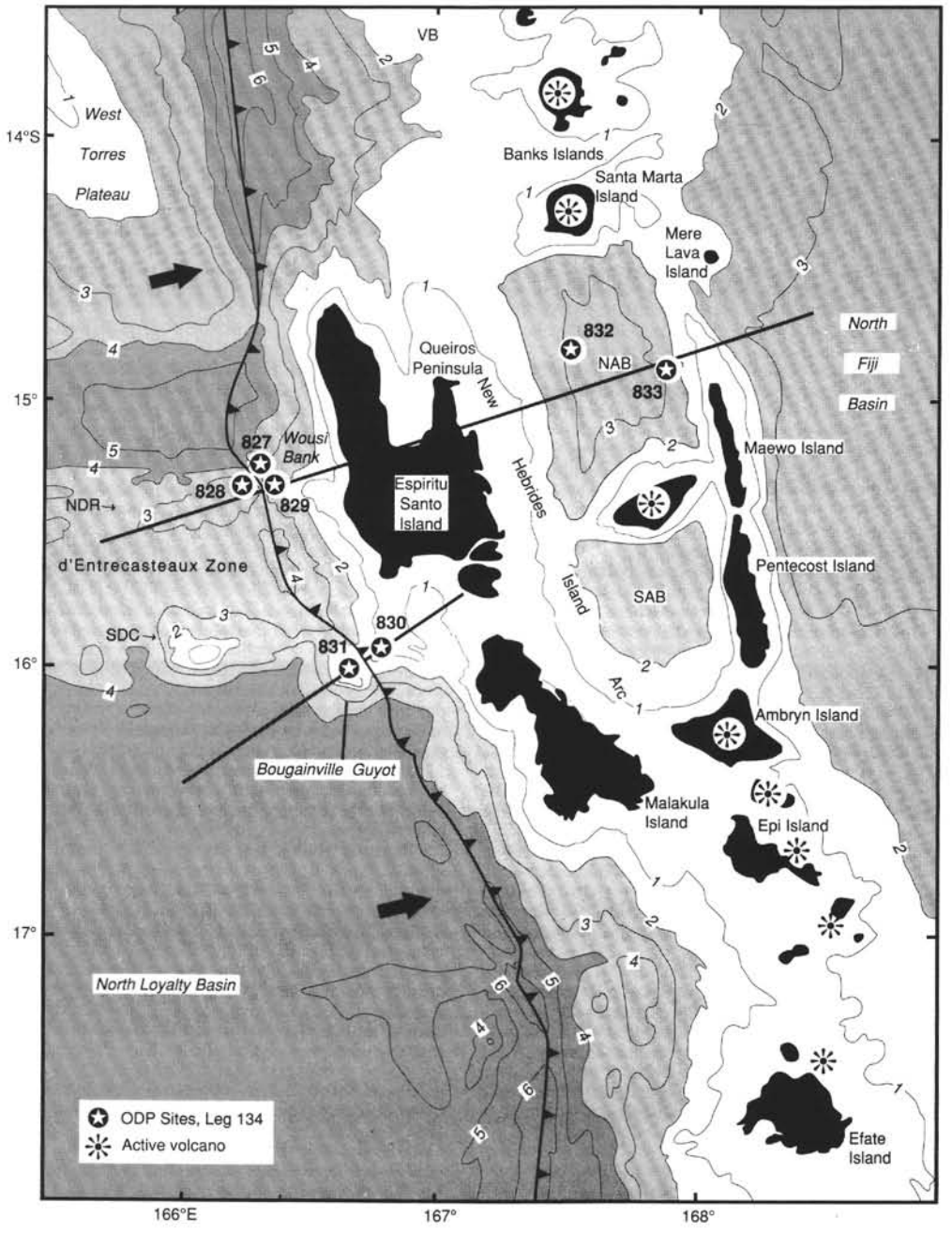

Figure 1. Map of the central New Hebrides Island Arc showing Leg 134 drill sites. Bathymetry in kilometers. NDR = North d'Entrecasteaux Ridge; SDC = South d'Entrecasteaux Chain; NAB = North Aoba Basin; SAB = South Aoba Basin. Bold line with teeth indicates approximate position of subduction zone; teeth are on upper plate. Arrows indicate direction of plate convergence. From Collot, Greene, Stokking, et al. (1992).

circulation and identifying the origins and estimating the quantity of the externally derived fluids.

METHODS AND SAMPLE HANDLING

The pore fluids were separated from the sediment by squeezing 5- to 35-cm lengths of the whole round core in a mechanical vice at pressures up to 2 x 10^8 Pa. Based on visual inspection, portions of each solid sample that appeared to be contaminated with drilling fluid (surface seawater) were physically separated from the pristine sediment. Some samples were collected and squeezed but were too contaminated for use in this study; these are listed in Collot, Greene, Stokking, et al. (1992). After separation, the fluid was filtered through a 0.45 µm filter prior to storage or analysis. A portion of the separated fluid was used for shipboard measurements of Cl, Na, Ca, Mg, NH_4, PO_4, Si, SO_4, pH, alkalinity and salinity concentrations, and the remaining fluid was archived for future shore-based analytical work. The sampling procedure is described by Collot, Greene, Stokking, et al. (1992). The techniques used for shipboard analyses are standard shipboard procedures described by Gieskes et al. (1992).

The shore-based geochemical analyses include measurements of the pore-fluid concentrations of Li, Sr, Br, I, and B from all seven

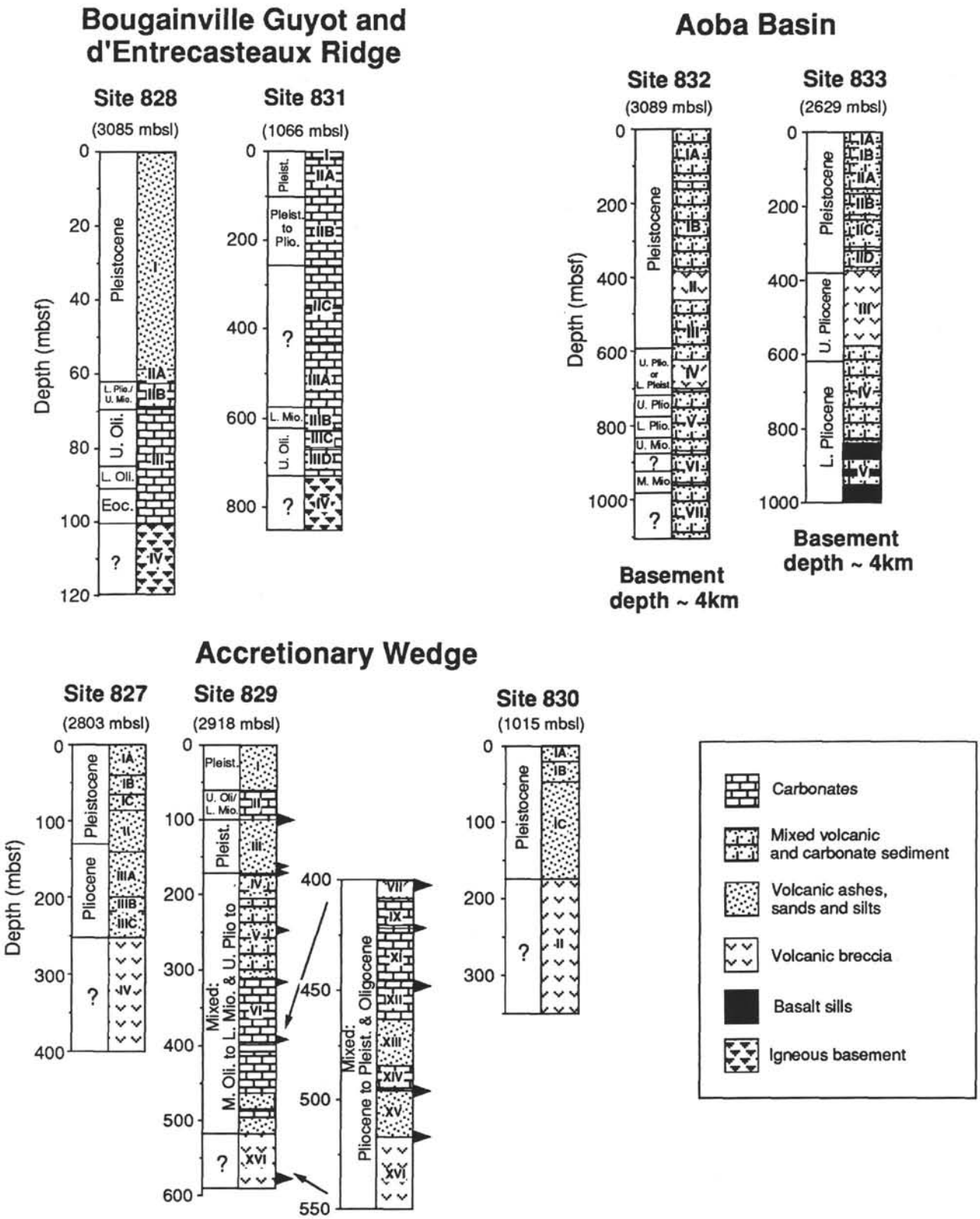

Figure 2. Schematic diagram of general lithologies and sedimentary units at the New Hebrides Island Arc. Water depth for each site, shown as meters below sea level (mbsl), is the average of the water depths of all holes at each site. At Site 829 large arrows indicate major thrust faults; small arrows indicate minor thrust faults. Units VIII and X are 0.4 and 5.7 m thick, respectively, and are not shown. Data taken from Collot, Greene, Stokking, et al. (1992).

sites. The $^{87}Sr/^{86}Sr$ ratios of dissolved Sr and $\delta^{18}O$ and δD values of the water were measured for Sites 827 and 829 in the accretionary wedge and for Site 833 in the Aoba Basin. The Li and Sr concentrations were measured by flame atomic emission and absorption spectroscopy respectively, Br concentrations by an iodiometric titration, and the I and B concentrations spectrophotometrically (Gieskes et al., 1992). Based on repeated measurements of either IAPSO or La Jolla Pier Water used as internal standards, the precision of all solute measurements is within ±4% (2σ). The $^{87}Sr/^{86}Sr$ ratios were measured at Scripps Institution of Oceanography with standard values of 0.710265 for NBS 987 and 0.709175 for North Atlantic and Central Pacific seawater. Repeated measurements of these standards yield a standard error of $\pm 22 \times 10^{-6}$ (2σ). The δD and $\delta^{18}O$ values were measured at Global Geochemical Corporation and are reported relative to the SMOW standard with errors of ±1.5‰ (2σ) for the δD values and ±0.1‰ (2σ) for the $\delta^{18}O$ values.

The mineralogical compositions of selected bulk sediments from Sites 829, 832, and 833 were determined by X-ray diffraction techniques (Cu K_α radiation) using aliquots of the sediments from which the pore fluids had been extracted. No treatments were applied to the sediments prior to the analyses. The relative mineralogical abundances in each sample were qualitatively estimated based on the major peak heights of each mineral.

RESULTS

The concentrations of all the measured solutes from each site are given in Table 1, which reports the concentrations at the North d'Entrecasteaux Ridge (NDR) and Bougainville Guyot Sites 828 and 831, the concentrations at the North Aoba Basin Sites 832 and 833, and the concentrations at the accretionary wedge Sites 827, 829, and 830. Figure 3 shows the depth profile at the NDR Site 828, but because only two samples were collected from the Bougainville Guyot (Table 1, Sites 828, 831), these data are not plotted vs. depth. Table 2 reports the δD and $\delta^{18}O$ values of water and Table 3 reports the $^{87}Sr/^{86}Sr$ ratios of dissolved Sr at Sites 827, 829, and 833. Based on the results of X-ray diffraction measurements, bulk mineralogy of selected samples are reported in Table 4.

DISCUSSION

North d'Entrecasteaux Ridge and Bougainville Guyot (Sites 828 and 831)

Site 828, drilled on the crest of the NDR (Fig. 1), is a reference site designed to provide information about the sediments approaching the subduction zone. The objectives of this site were to document transfer of material from the subducted to the overriding plate and to observe whether fluids flow from the accretionary wedge into sediments seaward of the deformation front. Similarity between sediments found at Site 828 and the accretionary wedge Site 829 (Fig. 2) suggests that sediment has been transferred from the ridge into portions of the accretionary wedge (Collot, Greene, Stokking, et al., 1992; Reid et al., this volume). At Site 828, solute concentrations vary only slightly from seawater values (Fig. 3) and these compositional changes can best be explained as a result of various diagenetic reactions. At shallow burial depths (<18.4 meters below seafloor [mbsf]), maxima in NH_4, alkalinity, and phosphate, and a slight decrease (to 26.3 mM) in the SO_4 concentration demonstrate minor organic carbon diagenesis. At greater burial depths (below 50 mbsf) decreasing Mg and increasing Ca concentrations indicate reaction with the basement rocks or ash, typical of the alteration from basalt to clay minerals (McDuff and Gieskes, 1976; Lawrence and Gieskes, 1981; Gieskes, 1981). These reactions could also be responsible for the decreasing K and Na concentrations. The Sr concentration increases from the sediment/water interface to the basement. This increase is sharpest in the deepest two samples reflecting the increasing sedimentary carbonate content (Fig. 2). The Li and B concentrations exhibit shallow minima that could reflect uptake reactions during ash diagenesis. None of these changes in the pore-fluid chemistry could be attributed to flow of fluid from the accretionary wedge. No section of tectonized sediment was observed which would indicate the location of the proto-decollement and the likely flow horizon for accretionary wedge fluids. In contrast to the New Hebrides margin, at the Barbados margin chemical characteristics of fluids recovered from the proto-decollement zone and from sand layers below the proto-decollement seaward of the deformation front suggest that there is active flow from the accretionary wedge (Moore, Mascle, et al., 1987; Blanc et al., 1988; 1991; Gieskes et al., 1990; Vrolijk et al., 1990, 1991).

The Bougainville Guyot site (831) was plagued by limited core recovery and thus only two pore-fluid samples were collected from the 727-m thick carbonate cap (Fig. 2). These samples are characterized by solute concentrations that are close to seawater values, with the exception of elevated Sr concentrations of 136.7 μM at 3 mbsf and 212.8 μM at 135 mbsf (Table 1). These concentrations probably reflect recrystallization of carbonate, also observed by Quinn and Taylor (this volume). Even the shallowest fluid sample is characterized by a Sr concentration 56% greater than seawater value, suggesting there is a diffusive Sr flux upward through the guyot.

North Aoba Basin (Sites 832 and 833)

Diagenetic and Temperature Controls of Mineral Authigenesis and Solute Concentrations

In the North Aoba Basin Sites 832 and 833, all pore fluid solutes show large deviations from seawater concentrations (Figs. 4 and 5). The sediment contains an average of <0.5 wt% organic carbon (Collot, Greene, Stokking, et al., 1992), and at burial depths above 100 mbsf where the sediment was deposited at rates >300 m/m.y., maxima in the alkalinity, PO_4, NH_4, and I concentrations and a corresponding SO_4 minimum reflect organic carbon diagenesis. In only a few samples at Site 833 is SO_4 reduction complete, and at Site 832 the SO_4 minimum reaches values of only 0.6 mM (Table 1). Below these minima, the concentrations increase to maxima of around 23.8 mM (Site 832) and 14.6 mM (Site 833), approaching but never reaching seawater concentration. At the depths of the SO_4 maxima, the sedimentary organic-carbon contents are often <0.1 wt% (Collot, Greene, Stokking, et al., 1992) and the PO_4 and NH_4 concentrations are low—less than 1 μM and 350 μM, respectively (Figs. 4 and 5). These low organic carbon, PO_4, and NH_4 concentrations imply that there has been little organic carbon available for diagenesis, hence minor SO_4 reduction. The SO_4 maxima thus could be caused by trapping of seawater sulfate in organic carbon-poor sediment. Sediment between the SO_4 maxima and minima was deposited in less than 1 m.y. (Collot, Greene, Stokking, et al., 1992), and thus little SO_4 has diffused into the overlying, more organic carbon-rich sediment.

Sediments at those burial depths with SO_4 maxima correspond to lithostratigraphic units composed principally of volcanic breccias: Units II and IV at Site 832 and Unit III at Site 833 (Fig. 2), which diluted to even lower values the small quantities of detrital organic matter found in the other units. Similar to the diagenesis attributed to basement reactions on the NDR, diagenesis of the volcanic breccia strongly alters the alkali and alkaline earth-element concentrations. Because the sediment thickness in the North Aoba Basin reaches a maximum of 4 km (Pontoise et al., this volume), this diagenesis must result from reactions within the sediments. The amount of volcanic material and the sedimentation rates are greater in the North Aoba Basin than on the NDR, and thus the solute concentrations are more altered in the North Aoba Basin. Within the volcanic breccia units the pore fluid contains no measurable Mg, the Na and K concentrations decrease to minimum values (Table 1; Figs. 4 and 5), and Ca concentrations increase to maxima of 216 mM and 549 mM at Sites 832 and 833, respectively. Above the breccia units, the Na and K concentrations are greater than seawater values by up to 16% and 52%, possibly representing leaching of these elements from the ash at low tempera-

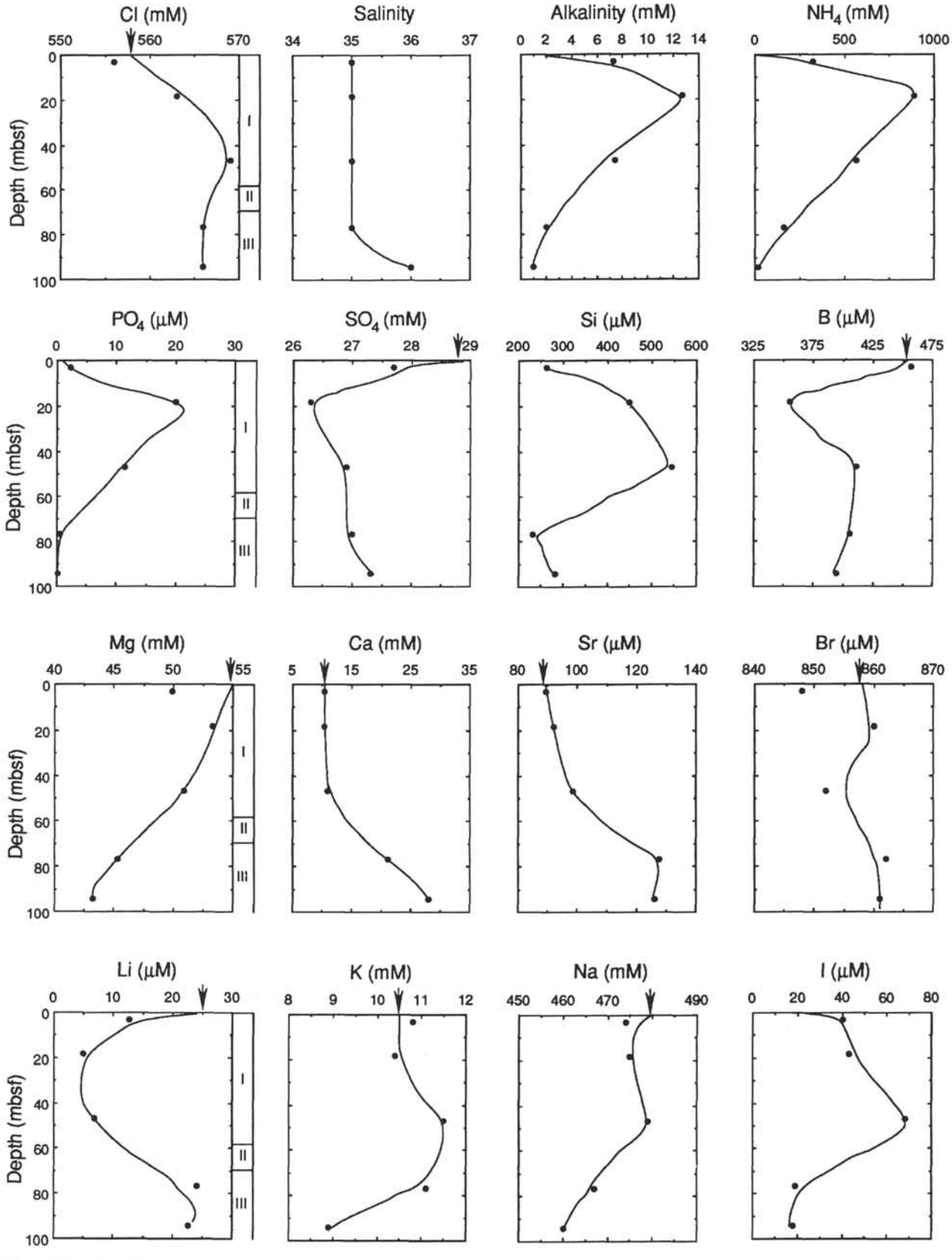

Figure 3. Depth profiles of pore fluid species and unit thicknesses for North d'Entrecasteaux Ridge Site 828. Arrows indicate seawater composition.

Table 1. Pore fluid solute concentrations for Sites 827, 828, 829, 830, 831, 832, 833.

Core, section, interval (cm)	Depth (mbsf)	Cl (mM)	Salinity	Alkalinity (mM)	pH	NH_4 (μM)	PO_4 (μM)	SO_4 (mM)	Si (μM)	B (μM)	Mg (mM)	Ca (mM)	Sr (μM)	Li (μM)	Na (mM)	K (mM)	Br (μM)	I (μM)
134-828A-																		
1H-2, 145–150	3.0	556	35.0	7.3	7.8	323	2.3	27.7	263	457	49.9	10.4	89.5	12.6	474	10.8	848	40
3H-3, 145–150	18.4	563	35.0	12.7	7.9	888	20.0	26.3	449	355	53.3	10.4	92.0	5.0	475	10.4	860	43
6H-3, 145–150	46.9	569	35.0	7.4	7.6	567	11.4	26.9	545	411	50.9	10.9	98.6	6.8	479	11.5	852	68
9H-5, 145–150	76.9	566	35.0	2.0	7.6	161	0.5	27.0	232	406	45.3	21.1	127.6	24.1	467	11.1	862	19
134-828B-																		
1R-3, 135–150	94.4	566	36.0	1.0	7.5	18	0.2	27.3	282	394	43.2	28.0	125.9	22.6	460	8.9	861	18
134-831A-																		
1H-2, 145–150	3.0	559	35.0	3.0	7.7	5	0.9	28.5	210	392	55.8	10.7	136.7	34.1	469	10.4	861	8
134-831B-																		
5R-3, 145–150	135.4	559	37.0	3.0	7.7	27	0.3	27.8	134	373	53.3	11.4	212.8	31.5	470	10.6	847	5
134-832A-																		
1H-3, 145–150	4.5	551	34.5	4.9	7.9	71	12.0	26.1	396	396	50.6	9.3	84.6	24.2	477	12.1	841	20
4H-3, 145–150	23.0	560	35.1	23.0	7.8	1336	75.0	4.5	425	453	46.1	3.0	48.0	18.7	486	11.7	898	46
6H-3, 145–150	42.0	566	34.0	28.0	8.0	1680	99.7	0.6	437	452	47.3	1.9	46.5	15.9	483	10.8	879	60
8H-2, 144–150	59.5	568	34.0	30.0	8.1	1973	104.5	0.7	425	440	46.7	2.3	47.2	14.2	484	10.9	872	67
10H-3, 143–150	77.0	566	34.0	30.0	8.1	2307	119.8	0.8	542	525	43.8	2.2	44.1	14.3	489	10.3	859	72
16H-3, 145–150	117.5	573	34.0	27.3	7.8	2291	89.3	0.8	484	470	42.3	2.3	45.7	16.4	489	9.6	879	74
19H-1, 145–150	142.5	577	34.0	26.3	8.0	2246	86.4	1.2	530	435	42.6	2.5	48.0	17.1	490	9.7	880	70
24H-2, 145–150	180.7	583	34.5	21.7	7.8	1897	42.5	2.4	501	400	42.7	3.4	61.3	26.9	495	9.2	897	65
134-832B-																		
9R-2, 140–150	222.9	596	34.2	11.0	8.0	2054	14.8	0.6	458	345	35.5	4.7	77.6	18.8	499	10.8	888	74
15R-2, 58–68	280.0	622	36.0	0.7	8.2	1599	1.0	2.9	316	218	14.2	30.6	243.2	26.3	501	15.2	931	65
17R-1, 10–20	300.3	642	38.0	0.5	7.9	1159	0.7	4.8	389	169	15.7	54.5	479.4	34.8	484	12.6	980	66
19R-1, 140–150	319.5	673	41.0	0.5	7.8	693	0.7	7.9	446	218	12.1	102.3	849.6	53.2	443	9.1	993	61
21R-3, 140–150	341.8	700	45.0			203		12.8	473		0.0	168.3			392	4.4		
23R-2, 16–31	358.2	692	45.0	0.4	8.1	168	0.5	13.8	511	255	0.0	177.3	511.3	55.7	363	3.9	1020	43
28R-2, 135–150	407.8	674	46.3	0.9	8.9	46	0.5	17.0	121	291	0.0	192.4	434.7	50.7	344	2.3	1004	28
30R-4, 138–150	428.0	653	43.2	0.5	8.5	142	0.5	21.5	389	238	0.0	140.8	1015.5	54.0	410	4.8	984	24
32R-2, 135–150	445.8	645	42.2	0.3	8.3	261	0.5	22.0	477	258	2.9	116.7	1104.9	53.3	441	6.8	982	25
34R-1, 135–150	462.9	645	42.0	0.3	8.3	429	0.5	22.0	379	222	2.5	97.4	1130.4	49.3	477	8.9	954	22
37R-3, 130–150	494.7	637	41.0	0.3	8.1	386	0.5	22.0	404	248	3.3	90.5	1098.5	47.7	488	8.3	955	23
40R-1, 123–135	520.7	655	44.0			323		23.8	358	290	7.8	85.1	970.9	50.1	488	7.9	979	23
42R-2, 0–13	540.4	674	42.5	0.4	8.1	261	0.5	23.4	429	314	2.7	110.3	1162.4	56.7	481	6.4	1003	24
45R-1, 130–150	569.0	698	46.2	0.3	6.7	301	0.5	21.3	439	319	0.9	148.4	1373.0	75.7	447	5.7	1036	25
47R-1, 130–150	588.3	719	48.0	0.4	7.7	203	0.5	20.4	282	304	3.3	166.8	1277.2	77.8	415	5.1	1021	26
49R-CC, 0–20	611.2	742	50.6	0.3	8.0	145	0.5	16.5	408	412	0.5	215.9	964.5	81.0	344	4.0	1040	25
59R-3, 130–150	706.3	708	48.5	0.1	7.9	272	0.5	14.5	586	165	3.2	180.2	1207.0	71.1	374	4.3	1034	25
61R-2, 130–150	723.6	682	45.1	0.3	8.2	349		14.6	270	135	3.9	150.6	1839.0	86.8	401	4.2	996	25
63R-6, 0–20	747.3	678	44.2					14.4							432	4.1		
66R-3, 130–150	773.1	631	40.0			298		19.9	156	283	9.2	98.4	1609.2	69.3	448	4.2	935	34
69R-4, 0–20	802.3	680	44.0			352		22.9	230	155	10.1	122.8	1373.0	70.4	462	3.9	990	41
72R-4, 127–146	832.8	704	46.0			207		20.8	150	216	0.0	147.0	875.1	66.9	450	3.6	1012	46
134-833A-																		
1H-3, 145–150	4.5	568	34.0	14.0	8.0	651	51.3	8.4	404	450	39.7	4.3	69.6	19.8	488	12.0	873	40
3H-3, 145–150	23.5	596	35.0	19.9	7.8	1645	55.2	0.0	391	442	35.5	2.6	65.3	12.3	506	11.7	901	78
6H-1, 145–150	40.7	603	35.0	16.9	8.1	1794	41.1	0.6	307	410	34.3	3.0	67.9	11.8	503	11.9	941	75
8H-1, 145–150	55.5	613	36.0	14.4	8.0	1596	30.0	0.0	399	411	31.8	3.0	68.8	14.9	507	12.1	962	77
10H-4, 145–150	68.9	617	36.0			1690	20.8	0.0	366	361	29.8	3.5	73.9	15.2	508	12.2	923	75
13H-1, 145–150	79.5	620	36.0	8.8	8.1	1491	18.8	0.7	319	372	29.1	4.8	103.3	18.6	518	14.2	944	74
16X-2, 140–150	95.6	636	36.3	2.7	8.2	1600	3.3	1.1	307	283	24.1	7.4	135.2	18.9	533	14.9	980	70
21X-2, 140–150	144.9	688	40.0	1.1	8.2	1466	1.9	3.3	292	253	25.9	15.6	219.9	25.7	512	12.9	1024	73
23X-2, 0–10	162.8	702	41.0	1.6	7.8	1273	1.9	5.1	370	290	35.0	22.1	342.9	31.6	534	14.6	1042	80
26X-1, 92–102	191.2	726	44.0	0.9	7.9	1223	1.9	7.2	378	316	35.5	43.1	810.3	53.2	521	14.2	1065	82
134-833B-																		
5R-2, 90–101	118.2	660	37.8	1.0	8.0	1364	0.8	2.4	310	270	21.3	14.9	191.4	21.4	522	14.7	997	69
16R-1, 140–150	223.5	761	46.3	0.5	7.8	855	0.6	10.3	464	355	35.1	88.7	2165.6	87.8	500	12.6	1089	89
18R-1, 141–150	242.3	771	48.0	0.4	7.8	741	0.4	11.9	443	331	31.7	109.6	2321.4	95.7	485	11.7	1102	76
20R-1, 140–150	261.4	830	50.0	0.1	7.6	667	0.4	12.3	498	358	30.7	135.7	2539.5	104.1	483	10.7	1118	77
22R-2, 0–10	280.8	884	58.2	0.3	7.9	469	0.4	14.6	334	384	11.5	227.9	2570.6	122.2	419	8.5	1179	77
25R-1, 95–105	309.2	956	65.0	0.4	8.0	231	12.0	14.4	387	330	1.6	316.7	2337.0	129.1	329	5.2	1260	91

tures. The subsequent decrease in their concentrations with depth probably reflects the conversion of ash into crystalline minerals during greater burial and increasing temperature and age. Lithium exhibits a behavior opposite to Na and K, initially decreasing below seawater values (minimum concentration 11.8 μM), but reaching maximum concentrations (129.1 μM) within the volcanic breccia units. These concentrations indicate a sedimentary sink for Li in the shallow sediments, but a source of Li in the deep sediments, probably caused by ash diagenesis and authigenesis of silicate minerals (e.g., Martin et al., 1991).

The most important hydrous mineral phases that are observed using X-ray diffraction analysis of bulk samples include clay minerals, chabazite, and analcite (Table 4) although more detailed X-ray diffractometry from Site 833 (Gerard and Person, this volume) show that other zeolite minerals are present. At shallow depths no zeolite peaks are present and clay peaks are small, but these minerals make up increasingly larger fractions of the sediment with depth (Table 4), suggesting that they are principally authigenic in origin. Although specific clay minerals have not been identified, a common, authigenic clay mineral is chlorite; its authigenesis along with analcite could cause the decrease in the pore fluid Mg and Na concentrations, respectively. Other authigenic silicate minerals could include quartz and feldspar, although quartz is only a minor component of the North Aoba Basin sediments (Table 4). Feldspars are the only crystalline phases contained in the two ash samples from Hole 833A, samples 2H-6, 50–60 cm, and 4H-6, 60–70 cm (Table 4). The proportion of detrital to authigenic feldspars is unknown, but feldspars dominate the bulk sediment at shallow depths where pore-fluid composition is

Table 1 (continued).

Core, section, interval (cm)	Depth (mbsf)	Cl (mM)	Salinity	Alkalinity (mM)	pH	NH_4 (μM)	PO_4 (μM)	SO_4 (mM)	Si (μM)	B (μM)	Mg (mM)	Ca (mM)	Sr (μM)	Li (μM)	Na (mM)	K (mM)	Br (μM)	I (μM)
134-833B-																		
27R-1, 136–150	328.9	1014	70.0	0.3	8.0	43	0.6	13.1	378	368	0.7	373.5	1651.5	127.6	284	3.2	1350	96
29R-1, 117–131	348.1	1042	72.0	0.5	8.4	48	0.4	13.9	414	436	0.0	399.5	950.5	115.4	237	3.6	1380	104
31R-2, 135–150	369.1	1015	72.0	0.3	8.0	48	0.6	13.3	382	344	0.0	389.0	997.2	116.6	242	2.5	1345	100
33R-1, 112–125	386.3	988	69.5	0.4	8.5	0	0.4	12.2	85	357	0.0	381.0	374.1	97.0	228	1.5	1367	99
38R-4, 135–150	439.3	1141	81.5					12.7				491.6			187	0.7		
46R-3, 135–150	494.5	1241	88.3	0.5	8.6	0	0.4	12.0	160	521	0.0	548.5	132.7	118.1	197	0.7	1574	110
55R-4, 10–30	583.8	960	71.0					10.4				407.6			163	0.4		
60R-5, 0–18	631.4	908	65.0					5.4		404		385.2	131.8	96.4	150	0.8	1272	152
63R-2, 0–15	656.4	851	60.0	0.2	8.0	0	0.4	6.2	173	427	8.1	349.4	67.8	88.3	166	1.3	1240	135
66R-4, 0–15	688.3	828	59.0			0	0.4	5.6	137	319	4.4	336.9	185.3	85.7	168	0.8	1141	136
69R-2, 0–15	713.7	805	57.0					6.0				299.3			186	0.7		
74R-2, 130–150	763.6	719	57.5					7.3	130			213.3			276	1.3		
134-827A-																		
1H-4, 145–150	6.0	561	38.5	18.2	7.9	789	3.3	30.5	349	448	60.9	11.7	53.8	6.8	488	11.8	833	170
3H-4, 145–150	25.3	580	36.0	15.0	7.8	1441	6.6	24.1	298	296	71.7	9.8	92.1	4.7	468	10.3	846	391
6H-4, 145–150	50.9	598	35.0	23.6	8.0	1925	18.2	0.0	352	350	66.0	7.0	89.6	3.3	455	11.4	893	400
9H-2, 145–150	70.0	596	35.5	18.7	7.9	1839	7.1	0.0	543	401	59.4	10.3	93.0	4.3	474	10.6	892	240
13H-2, 135–140	90.8	600	35.0	2.3	8.1	1337	1.9	1.0	356	378	41.0	21.4	117.6	14.6	475	13.2	897	122
134-827B-																		
2R-3, 145–150	122.1	604	38.5		8.0	1400	1.3	5.7	459	294	36.7	49.6	165.3	18.8	434	12.9	897	89
5R-2, 140–150	149.5	614	38.0	0.4	7.3	835	0.6	6.7	511	252	29.2	99.4	179.7	34.8	359	12.5	888	81
8R-4, 140–150	181.4	628	40.0			691		3.3	453		13.2	157.0			277	10.9		
11R-1, 135–150	205.9	622	40.0	0.1	6.8	841		3.2	356		9.3	175.8			248	9.0		
14R-2, 0–30	236.3	606	40.0	0.5	8.3	454	0.6	8.7	270	286	9.8	172.3	126.2	47.1	253	6.3	898	52
134-829A-																		
1R-1, 146–150	1.5	558	35.0	5.9	7.8	246	13.2	26.6	422	421	45.0	9.3	82.9	8.2	487	11.3	860	21
3R-2, 145–150	15.3	561	35.5	9.0	8.0	676	12.9	20.0	450	397	42.2	8.9	82.9	5.7	488	11.6	861	36
5R-5, 145–150	38.5	561	34.0	5.0	7.8	729	5.8	19.6	543	441	38.0	11.1	150.8	9.3	490	10.7	874	48
7R-1, 145–150	52.3	562	34.0	2.2	7.8	459	1.3	23.4	501	441	34.6	14.6	396.2	19.3	485	10.6	878	45
12R-5, 140–150	104.9	564	32.5	14.3	8.0	1319	24.4	0.6	531	374	38.9	4.8	75.5	5.5	477	10.4	876	95
14R-4, 135–150	124.1	568	32.5	12.0	8.0	1482	24.3	3.5	475	347	37.2	5.0	68.8	4.7	482	10.3	860	83
16R-4, 135–150	143.4	565	33.0	7.7	8.1	1521	11.0	10.6	527	362	35.8	7.3	108.6	5.9	482	11.0	870	64
18R-3, 135–150	161.2	564	34.0	4.4	8.2	1163		17.2	482	375	34.4	12.3	213.7	9.3	479	10.6	849	53
20R-2, 130–150	178.9	565				674		23.3	283	360	38.2	15.6	440.7	16.9	470	10.1	867	37
44R-1, 123–140	417.8	424						12.2			16.5				396	7.7		
56R-3, 130–150	517.7	709						4.5			20.2		61.0		362	7.2	636	
57R-2, 0–33	515.0	417						7.3			21.5		75.4		365	7.6	653	
134-829B-																		
2H-2, 145–150	3.5	554	34.5	6.6	7.9	403	16.1	18.8	334	456	42.6	9.2	81.3	4.9	470	11.3		32
134-829C-																		
1H-2, 145–150	3.0	556	35.0	6.8	7.9	417	12.2	22.2	341	424	42.9	9.0	84.6	4.9	472	11.7		23
1H-4, 145–150	6.0	556	35.0		7.9	781	17.0	17.0	416	416	42.7	8.6	82.9	4.7	484	10.5	856	35
2H-2, 145–150	9.8	556	34.5		7.9	987	20.3	13.0	440	389	41.1	7.8	82.5	5.0	484	10.4	860	46
3H-6, 135–140	26.8	558	34.0	7.7	7.8	907	12.9	13.3	458	412	36.2	8.4	94.5	6.5	472	11.6	865	58
134-830A-																		
1H-3, 145–150	4.5	552	35.0	3.7	7.9	216	4.8	22.8	456	338	46.4	8.4	85.3	16.8	469	12.0	860	17
3H-4, 145–150	22.5	564	32.0	2.7	7.8	605	1.8	4.9	319	415	38.1	8.2	91.3	7.5	467	10.6	876	55
5H-1, 145–150	36.4	568	32.0	2.5	8.1	952	1.8	4.1	319	313	35.8	10.3	103.2	6.5	456	9.1	894	81
134-830B-																		
2R-1, 140–150	59.5	575	32.0			1518	0.9	1.3	300	290	33.8	21.7	118.5	9.8	448	6.4	912	140
4R-1, 100–110	78.5	577	32.5	1.2	8.2	1570	1.0	0.5	314	303	34.7	25.0	127.9	9.8	451	7.6	911	172
6R-1, 134–150	98.4	578	33.5	1.4	8.1	1547	0.8	1.4	338	349	38.3	24.8	125.3	10.5	439	7.3	931	183
8R-1, 134–150	117.8	584	34.0	1.7	8.0	1786	0.9	1.9	456	276	41.6	23.4	125.3	10.3	436	9.1	959	185
10R-2, 0–19	141.0	587	34.0	1.5	8.1	1849	0.9	1.7	453	267	41.7	28.9	142.3	14.1	429	10.0	922	200
12R-2, 0–18	156.8	597	34.0	1.3	7.9	1629	0.6	2.5	488	292	36.8	57.9	160.2	22.6	403	9.9	975	190
18R-1, 135–155	214.8	620	43.5			0	0.5	14.7	153	168	3.5	208.2	138.1	66.3	216	0.0	952	134
134-830C-																		
10R-2, 0–10	323.0	603	42.5															
12R-2, 28–53	341.2	613	42.0	0.4	8.1	5	0.5	9.5	137		0.0	229.2	58.9	58.9	172	0.0	943	85

not greatly altered from seawater value, suggesting that much of the feldspar is detrital.

The modern temperature gradients in the North Aoba Basin are 42°C/km at Site 832 and 67°C/km at Site 833 (Fig. 6A). Based on these gradients, and a bottom-water temperature of 3°C, Units II and IV at Site 832 reach temperatures of approximately 19°C and 25°C, respectively, and Unit III at Site 833 reaches a temperature of 34°C. Higher temperatures are probably responsible for more extensive diagenesis and thus the greater changes in pore-fluid composition at Site 833 than Site 832, but even the higher temperatures are lower than commonly assigned to metamorphic facies based on such authigenic mineral assemblages. Although the heat flow and geothermal gradients would have been greater during times of intrusion of the sills found at the base of Site 833 (Fig. 2), the modern pore fluid concentrations imply that the authigenic minerals are currently forming, even at these low formation temperatures. The sills were intruded at 3.3±0.3 and 3.65±0.18 Ma (Rex, this volume) under approximately 110 m of overlying sediment cover. Assuming an emplacement temperature of ~1500°C and based on thermodynamic data given in Robie et al. (1979) and the measured thermal conductivities (Collot, Greene, Stokking, et al., 1992), simple diffusion would have dissipated heat from the sill in $<10^4$ years. All sediment younger than 3.3 m.y. (shallower than ~700 mbsf) would be unaffected by this heat. In the absence of additional heat sources, the authigenic minerals would have formed at the relatively cool temperatures governed by temperature gradients similar to the modern ones (Fig. 6A).

An approximately linear exchange of Ca for Na, K, and Mg occurs in the pore fluids (Fig. 7A), but the slope of the line is not unity

Table 2. Stable isotope ratios of water.

Core, section, interval (cm)	Depth (mbsf)	$\delta^{18}O$ (‰)	δD (‰)
134-827A-			
1H-4, 145–150	6.0	–0.5	–5.0
6H-4, 145–150	50.9	–1.6	+3.0
13H-2, 135–140	90.8	–2.9	–3.0
143-827B-			
5R-2, 140–150	149.5	–4.2	–1.5
14R-2, 0–30	236.3	–5.0	+3.0
134-829A-			
1R-1, 146–150	1.5	–0.2	+2.5
5R-5, 145–150	38.5	–3.0	–1.0
7R-1, 145–150	52.3	–0.7	+5.5
12R-4, 140–150	104.9	+0.5	–1.5
16R-4, 135–150	143.4	–0.7	+1.5
20R-2, 130–150	178.9	–0.8	–3.0
56R-3, 130–150	508.1	–0.7	–8.0
57R-2, 0–33	515.0	–0.4	–5.0
134-833A-			
1H-3, 145–150	4.5	–0.9	–4.5
3H-3, 145–150	23.5	–2.2	+2.5
8H-1, 145–150	55.5	–2.7	+7.5
16X-2, 140–150	95.6	–3.5	+2.5
21X-2, 140–150	144.9	–4.2	–0.5
134-833B-			
16R-1, 140–150	223.5	–5.2	+2.5
22R-2, 0–10	280.8	–5.9	+0.5
33R-1, 112–125	386.3	–7.1	+2.5
46R-3, 135–150	494.5	–9.5	+8.5
63R-2, 0–15	656.4	–6.8	+2.0
66R-4, 0–15	688.3	–6.1	–2.5

Table 3. Strontium isotope ratios of dissolved Sr.

Core, section, interval (cm)	Depth (mbsf)	Sr (mM)	$^{87}Sr/^{86}Sr$
134-827A-			
1H-4, 145–150	6.0	53.8	0.708491
6H-4, 145–150	50.9	89.6	0.708038
13H-2, 135–140	90.8	117.6	0.708824
134-827B-			
5R-2, 140–150	149.5	179.7	0.708555
14R-2, 0–30	236.3	126.2	0.707828
134-829A-			
1R-1, 146–150	1.5	82.9	0.708743
5R-5, 145–150	38.5	150.8	0.708680
7R-1, 145–150	52.3	396.2	0.708489
12R-5, 140–150	104.9	75.5	0.708614
16R-4, 135–150	143.4	108.6	0.708536
20R-2, 130–150	178.9	440.7	0.708456
56R-3, 130–150	517.7	61.0	0.708493
57R-2, 0–33	515.0	75.4	0.708539
134-833A-			
1H-3, 145–150	4.5	69.6	0.708403
3H-3, 145–150	23.5	65.3	0.707871
8H-1, 145–150	55.5	68.8	0.707687
16X-2, 140–150	95.6	135.2	0.706870
21X-2, 140–150	144.9	219.9	0.707289
134-833B-			
16R-1, 140–150	223.5	2165.6	0.708790
22R-2, 0–10	280.8	2570.6	0.708653
33R-1, 112–125	386.3	374.1	0.707819
46R-3, 135–150	494.5	132.7	0.706064
66R-4, 0–15	688.3	185.3	0.706733

Note: All errors less than standard error except for Sample 833A-1H-3, which has an error of .000026.

Table 4. Bulk sediment X-ray diffraction results.

Core, section, interval (cm)	Depth (mbsf)	Major Mineralogy
134-829A-		
44R-1, 123–140	418	Calcite >>Feldspars >>Quartz
56R-3, 130–150	508	Calcite >Feldspars ≥Clays
57R-2, 0–33	515	Calcite >>Feldspars ≥Clays
134-832A-		
2H-6, 50–60	8	Feldspars
4H-6, 60–70	27	Feldspars
134-832B-		
15R-2, 58–68	280	Calcite >Feldspars >Quartz
21R-3, 140–150	342	Feldspars >Calcite >Clays
28R-2, 135–150	408	Feldspars > Chabazite ≥Clays
30R-4, 138–150	428	Calcite >Feldspars >Clays
32R-2, 135–150	446	Calcite >Feldspars
34R-1, 135–150	463	Calcite ~ Feldspars
40R-1, 123–135	521	Calcite >Feldspars >> Clays
134-833B-		
16R-1, 140–150	224	Calcite ~ Feldspars >> Clays
22R-2, 0–10	281	Calcite> Feldspars ~ Clays
27R-1, 136–150	329	Calcite ≥Feldspars >Clays
33R-1, 112–125	386	Analcite >Calcite >Clays ~ Feldspars
38R-1, 135–150	439	Feldspars >> Calcite
46R-3, 135–150	495	Calcite >Analcite >Feldspars ≥Clays
55R-4, 10–30	584	Calcite >Analcite >Clays ~ Feldspars
66R-4, 0–15	688	Analcite >Calcite >Clays >Feldspars
74R-2, 130–150	764	Calcite >Analcite >Clays >Feldspars

Note: Mineralogy is based on relative peak areas. No correction factors have been applied.

indicating that this exchange does not maintain the charge balance. The balance is maintained by changes in anion concentrations, principally Cl, although changes in the SO_4 concentration also are important (Fig. 7B). The changes in Cl concentration are extreme, reaching maxima of 742 mM at Site 832 and 1241 mM at Site 833 (Table 1). Other than during reactions with evaporite minerals such as halite, Cl should behave conservatively, in all common diagenetic reactions within marine sediments. In organic matter-poor sediments, Br also behaves conservatively, and thus during processes such as the early stages of seawater evaporation, the Br/Cl molar ratio should not change from the seawater value of 1.54×10^{-3}. The observed molar ratio of 1.05×10^{-3} (Fig. 8A) indicates that the high Cl and Br concentrations do not result from evaporation and that one or both of the ions are not conservative. The Br/Cl ratio is greater than expected from halite dissolution (e.g., Holser, 1966, 1970, 1979; Holser and Wilgus, 1981) and no evaporites have been observed at the New Hebrides Island Arc, indicating that evaporitic dissolution does not cause the high Cl concentrations. Alternatively, the high Cl and Br concentrations could be caused by removal of H_2O from the pore fluid during authigenesis of hydrous minerals. The conversion of ash into hydrous minerals could also alter the Br/Cl ratio depending on the unknown Br/Cl ratio in the ash, or by differences in distribution of Br and Cl into the authigenic minerals. Br/Cl molar ratios in typical andesitic lavas range from 1.5 to 6.3×10^{-3} (Gill, 1981, and references therein), considerably greater than seawater value, and should thus increase the pore-fluid Br/Cl ratio during dissolution. The Br/Cl ratio would decrease if Br has a greater distribution than Cl into authigenic minerals and much water is incorporated in the hydrous minerals as OH^-, likely structural sites for both Br^- and Cl^-. Because these ions have the same valence, their distributions would be controlled by size differences.

Assuming that the Cl concentrations increase solely from the transfer of water from the pore fluids into the authigenic, hydrous minerals, the mass of water, M_w, transferred per gram of sediment is

$$M_w = (1 - R_{Cl}) \cdot R_{wc}, \quad (1)$$

where R_{Cl} is the ratio of seawater Cl concentration to the measured pore-fluid concentration and R_{wc} is the ratio of the mass of pore water to the mass of the dry sediment taken from Collot, Greene, Stokking, et al. (1992). These calculations indicate that up to 0.2 g of water is incorporated per gram of sediment (i.e., 20 wt%). Because the Br/Cl

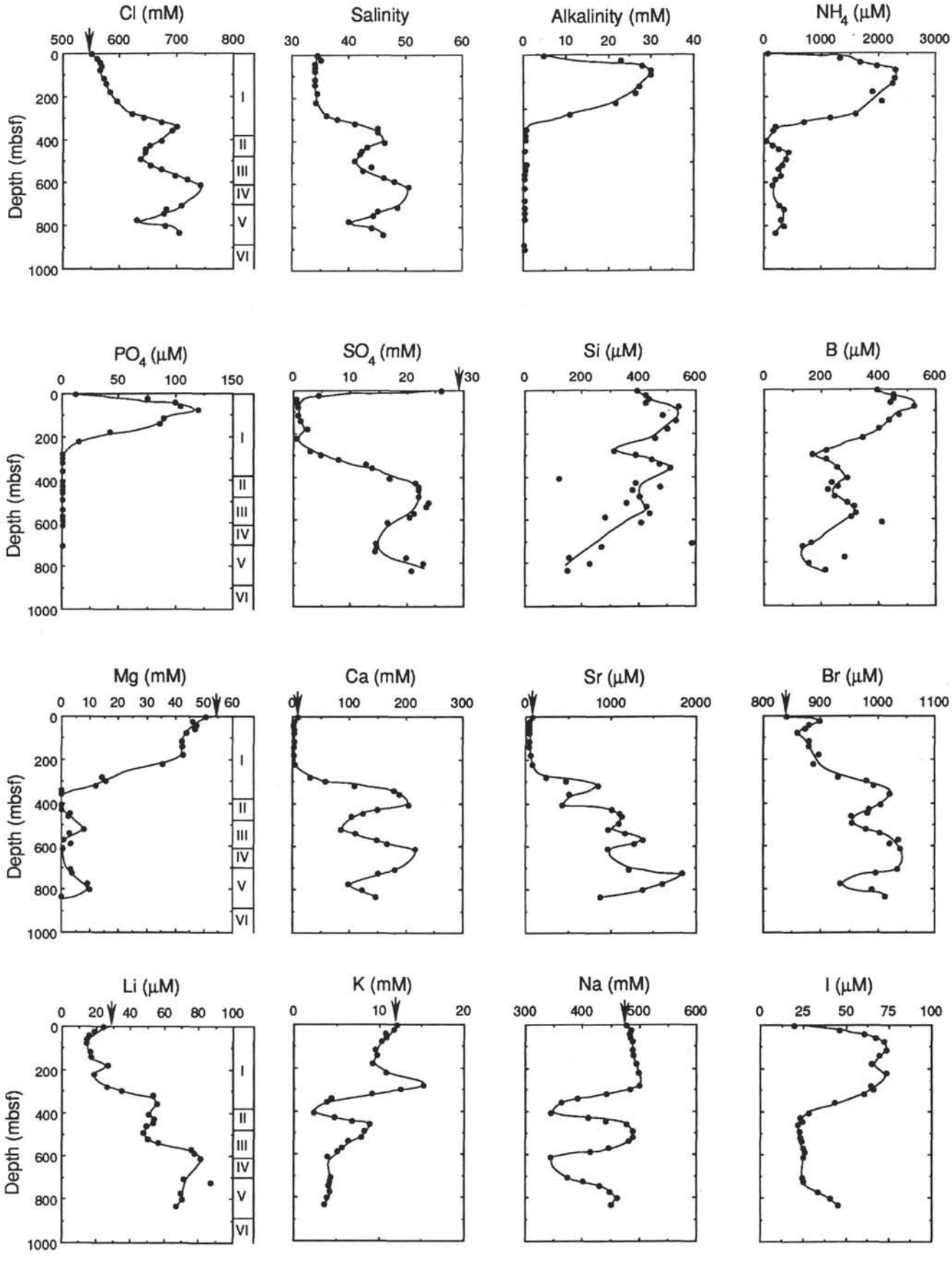

Figure 4. Depth profiles of pore fluid species and unit thicknesses for North Aoba Basin Site 832. Arrows indicate seawater composition.

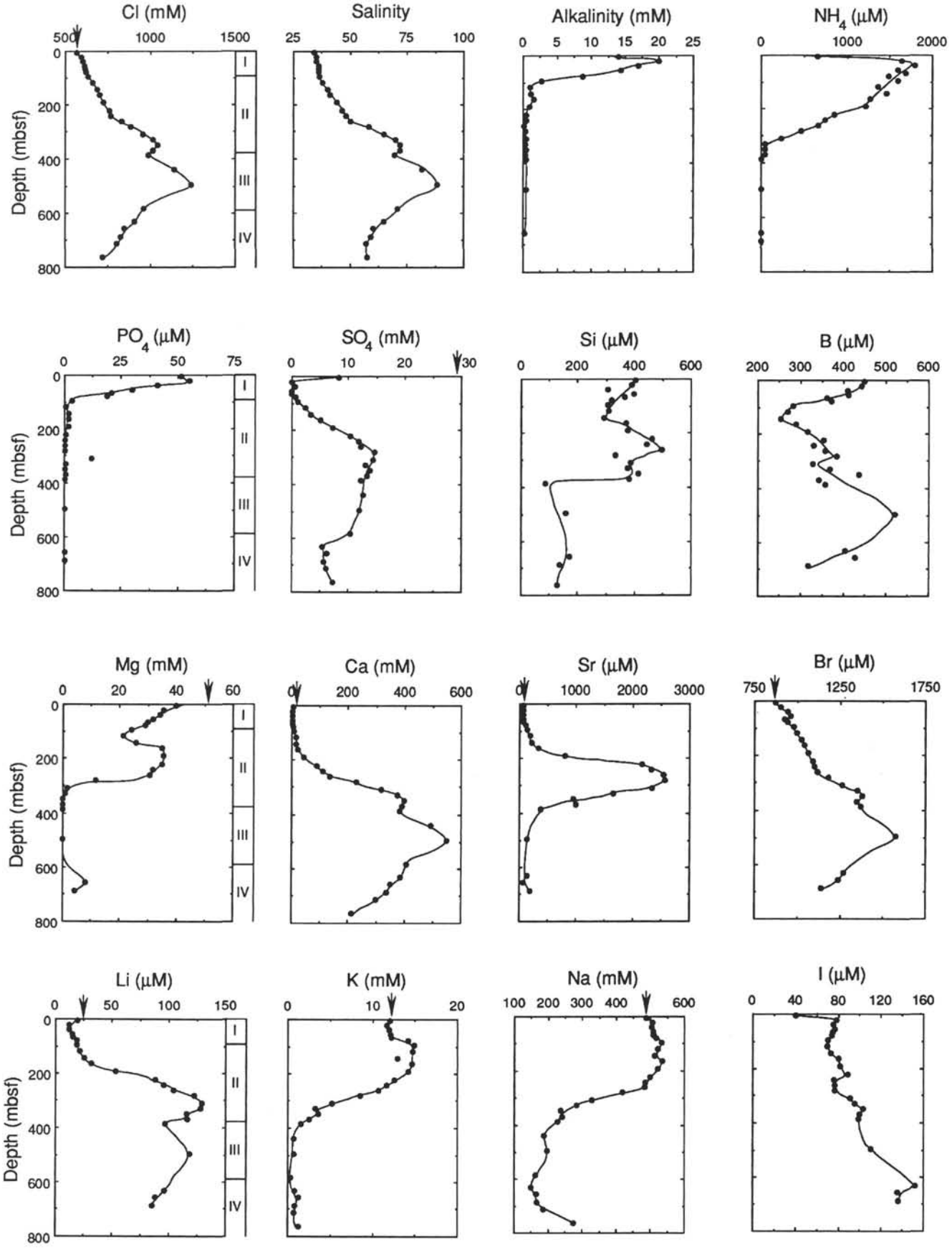

Figure 5. Depth profiles of pore fluid species and unit thicknesses for North Aoba Basin Site 833. Arrows indicate seawater composition.

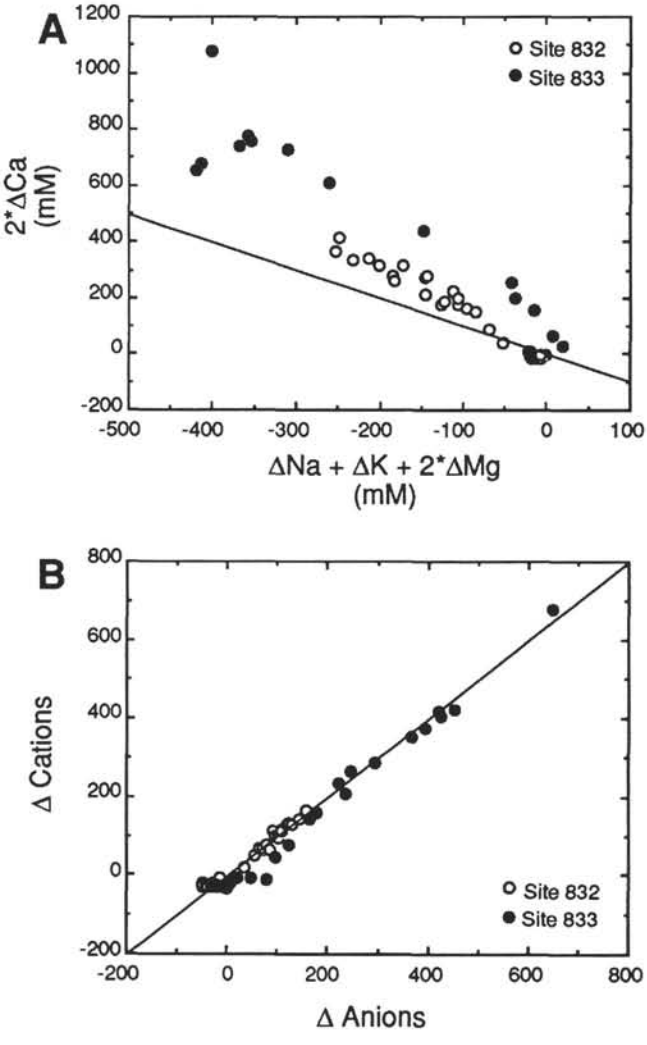

Figure 6. **A.** Plot of 2 ΔCa vs. sum of ΔNa + ΔK + 2 · ΔMg for the North Aoba Basin Sites 832 and 833. The Δ indicates the difference between the measured and seawater cation concentrations. The solid line indicates a slope of −1. **B.** Plot of the difference between the sum of the measured Na, K, Mg, and Ca concentrations and seawater concentrations vs. the difference between the sum of the Cl and SO_4 concentrations and seawater concentrations. The solid line indicates a slope of 1.

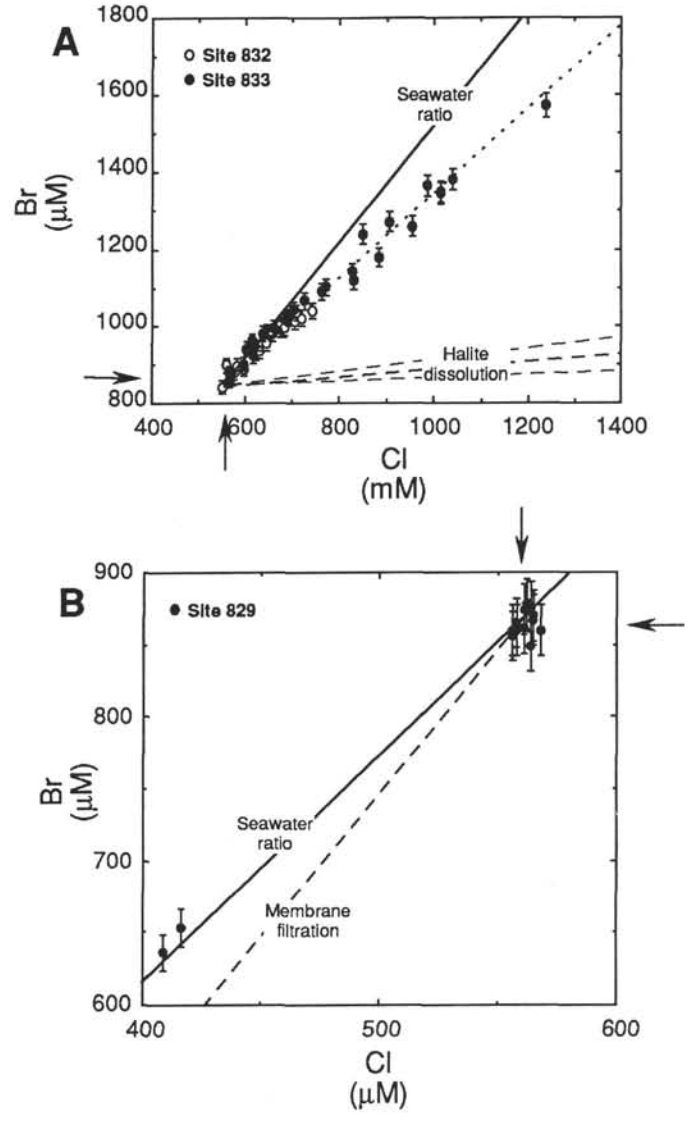

Figure 7. **A.** Plot of the Cl vs. Br concentrations from the North Aoba Basin Sites 832 and 833. The heavy dashed line indicates the Br/Cl ratio expected from dissolution of marine halite, and the light dashed lines indicate the possible range in Br/Cl ratio from this source. The heavy solid line indicates the Br/Cl ratio in seawater. The dotted line indicates the linear regression of all the data (n = 52, slope = 1.05 x 10^{-3}, r^2 = 0.98). **B.** Plot of the Cl vs. Br concentrations at accretionary wedge Site 829. The heavy solid line indicates seawater Br/Cl ratio. The dashed line indicates the Br/Cl ratio expected from membrane filtration based on results from Kharaka and Berry (1973). The arrows indicate seawater values.

ratio is ~32% lower than seawater value, a similar calculation based on Br concentration would indicate less water is incorporated into the sediments. The total water in clays and zeolites, including interlayer, channel and structural, ranges from 8 to 25 wt% (Sand and Mumpton, 1976; Newman, 1987), where the highest value is for smectite with three interlayer water molecules. The water contained in pure smectite is only slightly greater than the maximum value calculated from Equation 1, and therefore authigenesis of a pure smectite layer would be required to produce the maximum calculated level of hydration. Because the mineralogy in the North Aoba Basin is a mixture of clay and other minerals (Table 4), this calculated mass of water transferred is not supported by the mineralogy. In addition, because some Cl will diffuse from regions with maximum Cl concentrations and some Cl will be lost from the pore fluid due to its distribution into authigenic minerals, the imbalance between the calculated water lost from the pore fluids and the quantity of hydrous minerals available to incorporate the water must be even greater. This imbalance implies that there is a source of Cl in the sediments, which could be partly responsible for the observed low Br/Cl ratio (Fig. 7A).

The compositional changes in the major element concentrations (e.g., the exchange of Ca for Na, K, and Mg and the increase in the Cl concentrations; Fig. 6B) make these pore fluids $CaCl_2$ brines. Similar pore-fluid compositions have previously been reported from both convergent margins and deep ocean basin settings (Egeberg et al., 1990; Lancelot, Larson, et al., 1990; Chambers and Cranston, 1991; Blanc, Hawkins, Parsons, Allan, et al., 1991; Parsons, Hawkins, et al., 1992). These altered pore fluids typically reside in volcanic ash-rich sediment suggesting a mode of formation similar to the North Aoba Basin brines. The North Aoba Basin brines are the most extensively altered and occur in the youngest sediments of all the previously reported brines. At Site 832 the ages of Units II and IV are

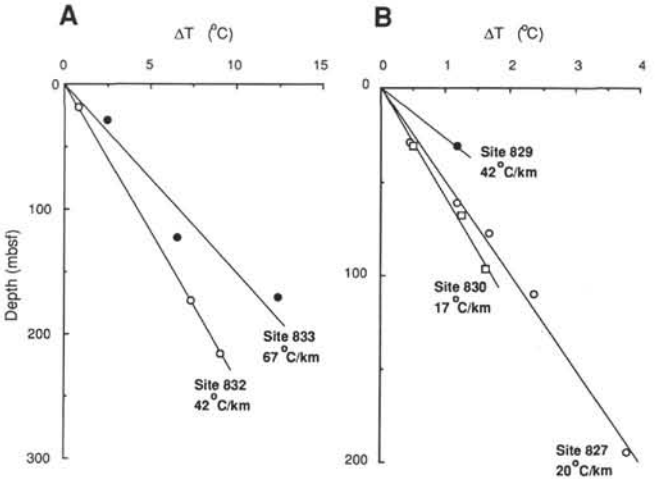

Figure 8. Temperature gradients from North Aoba Basin. (**A**) Sites 832 and 833, and (**B**) accretionary-wedge Sites 827, 829, and 830. The temperature values were measured using the WSTP tool and are taken from Collot, Greene, Stokking, et al. (1992). ΔT is the difference in the measured temperature from the bottom-water temperature.

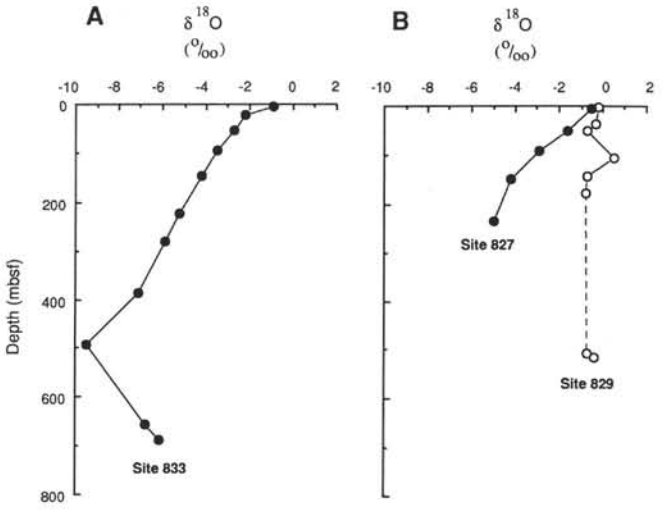

Figure 9. Depth profile of the $\delta^{18}O$ value of pore water at the North Aoba Basin, (**A**) Site 833, and (**B**) accretionary-wedge Sites 827 and 829.

between 0.45 and 1.45 Ma, and at Site 833 the age of Unit III is 1.57 to 1.89 Ma (Staerker, this volume). Assuming that the brines have not formed elsewhere and later flowed into the sediments, the ages of the sediment must be the maximum age of the brine. The young ages indicate that volcanic ash diagenesis and brine formation are very rapid processes.

Diagenetic Controls of Isotopic Compositions

Because the fractionation factor of oxygen between water and clay and zeolite minerals is >1, the alteration of ash to these hydrous minerals will decrease the $\delta^{18}O$ values of pore fluids in marine sediments (Lawrence et al., 1975; Lawrence and Gieskes, 1981). The decreasing $\delta^{18}O$ values with depth at Site 833 (Fig. 9A) support the interpretation based on the sediment and pore-fluid compositions of extensive ash alteration in the North Aoba Basin. The linear correlations between $\delta^{18}O$ values and Ca and Cl concentrations also indicate ash alteration, although there are abrupt changes in the slopes of both correlations at 144.9 mbsf (Fig. 10). Although at depths shallower than 144.9 mbsf Cl concentrations and $\delta^{18}O$ values correlate well, there is no correlation (r^2 = 0.22) between $\delta^{18}O$ values and Ca concentrations, indicating that different processes control these values in the shallow sediments. The changes in slope are unlikely to be caused by a temperature-dependent decrease in fractionation factor or a more rapid diffusion of oxygen than Ca or Cl because both processes would produce smoothly varying plots of $\delta^{18}O$ vs. Ca and Cl. The change in slope at 144.9 mbsf of the Ca-$\delta^{18}O$ plot is greater than the Cl-$\delta^{18}O$ plot and the linear correlation between Ca and Cl (Figs. 10C and 10D) also changes slope at this depth. The Ca concentrations at depths less than 144.9 mbsf are less than seawater value (Figs. 4 and 5) indicating possible uptake during precipitation of carbonate minerals, but where Ca concentrations increase rapidly at depths below 144.9 mbsf, ash diagenesis appears to be the dominant reaction. This switch from carbonate to ash diagenesis could result from the low alkalinities below 144.9 mbsf (Fig. 5), but could also be caused by a temperature dependent threshold for the conversion of ash into one or more of the authigenic minerals. The Ca-Cl correlations in Figure 10D indicate the change in slope occurs between 144.9 and 191.2 mbsf at Site 833, which suggests a range of 12.7 to 15.8°C, based on the temperature gradients shown in Figure 8A and assuming a bottom-water temperature of 3°C. The Ca-Cl correlation from Site 832 indicates the same change of slope, at greater depths between 222.9 and 280.0 mbsf, but at similar temperatures of 12.4 to 14.8°C. There is no lithostratigraphic change at these depths (Fig. 2), and although sedimentation rate decreases from 322 to 148 m/m.y. at 200 mbsf at Site 833, sedimentation rate is constant from the surface to 350 mbsf at Site 832 (Collot, Greene, Stokking, et al., 1992) suggesting that neither sediment composition or sedimentation rate control these profiles.

Although $^{18}O/^{16}O$ ratios of the pore water are extensively altered because of the diagenetic reactions, δD values differ only slightly from values for modern seawater (Fig. 11). Unlike oxygen, the isotopic fractionation of hydrogen between water and clay and zeolite minerals is controlled by a fractionation factor <1 (Savin, 1967). The difference in oxygen and hydrogen fractionation factors would increase the δD values and decrease the $\delta^{18}O$ values of the water, causing the values to plot to the left of the meteoric water line (Fig. 11). At Site 671 and 672, drilled at the Barbados margin, most of the stable isotope ratios also plot to the left of the meteoric water line (Vrolijk et al., 1990), suggesting that volcanic ash diagenetic reactions may be one important control of the stable isotope ratios of the water. At the Barbados forearc, however, the δD-$\delta^{18}O$ plot exhibits a positive slope that trends along the mean water level, or MWL (Vrolijk et al., 1990), unlike the New Hebrides plot, which exhibits the negative slope expected from volcanic ash diagenesis. The Barbados fluids thus may have a more complex origin than the New Hebrides fluids, including possible mixing with meteoric water.

Both carbonate diagenesis and volcanic ash diagenesis are reflected in the isotopic composition of Sr in the pore fluids at Site 833 (Fig. 12A). The volcanic ash in the North Aoba Basin has Sr isotope ratios of between 0.703 and 0.704 (Briqueu et al., this volume), thus the $^{87}Sr/^{86}Sr$ minima at 95.6 and 494.5 mbsf probably result from isotope exchange with this ash. At 233.5 mbsf the maximum in the $^{87}Sr/^{86}Sr$ ratio approaches the value for contemporaneous seawater and corresponds with a carbonate-rich zone containing up to 48 wt% $CaCO_3$ (Collot, Greene, Stokking, et al., 1992). The $^{87}Sr/^{86}Sr$ maximum also corresponds to a maximum in the Sr concentrations of 2570 μM (Fig. 5), which probably is due to diagenesis of the carbonate. At depths between 600 and 700 mbsf Unit IV also contains ~50% $CaCO_3$ (Collot, Greene, Stokking, et al., 1992), but the pore-fluid Sr concentrations and $^{87}Sr/^{86}Sr$ ratios remain low, suggesting the older carbonate may have recrystallized, exchanging its Sr isotopes.

Mixing between two end-member fluids with different Sr concentrations and isotope ratios results in an exponential mixing curve (see Faure, 1986, for derivation) that forms a straight line when the isotope

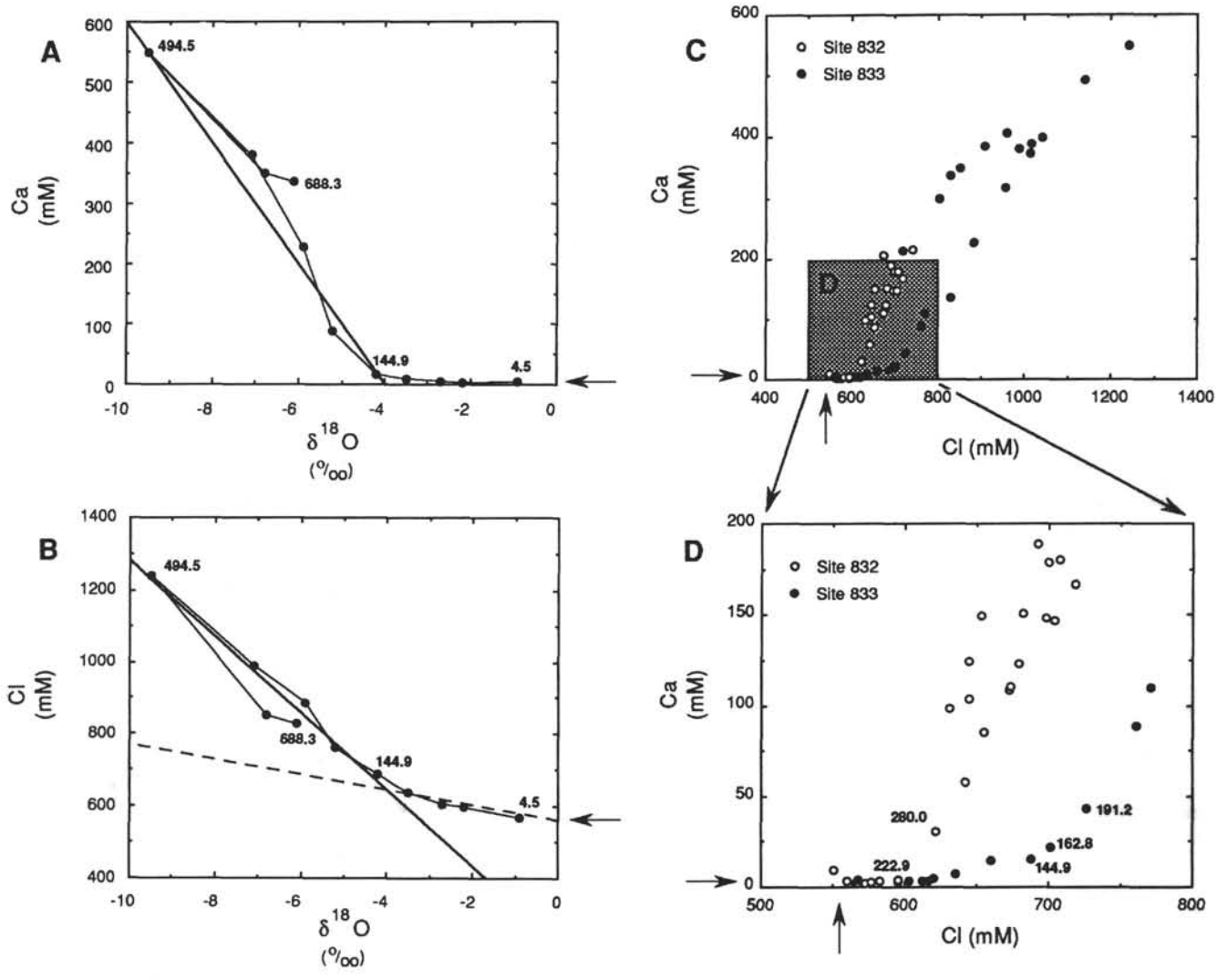

Figure 10. Plot of the $\delta^{18}O$ value of the pore water vs. **(A)** Ca concentration, and **(B)** Cl concentration for North Aoba Basin Site 833. The dashed line indicates the linear regression of the $\delta^{18}O$-Cl data from the shallow pore fluids ($n = 4$, slope = –26, $r^2 = 0.99$), the solid lines indicate the linear regressions of the $\delta^{18}O$-Cl and $\delta^{18}O$-Ca data from the deep pore fluids ($n = 7$, for A.: slope = –395, $r^{-2} = 0.94$; for B.: slope = –104, $r^2 = 0.94$). **C, D.** Plots of Cl vs. Ca concentrations for North Aoba Basin Sites 832 and 833. All data are plotted in **(C)**, while a selected range of data is plotted in **(D)** in order to emphasize the depth of the change in slope. The numbers beside the data in A, B, and D indicate the depth (mbsf) of selected samples. Arrows indicate seawater values.

ratios are plotted versus 1/Sr concentrations. At depths shallower than 144.9 mbsf such a plot is not linear (Fig. 13), indicating that the Sr concentrations and isotope ratios result from mixing of more than two end-members. Above 144.9 mbsf the pore-fluid Sr likely would be influenced by three sources: volcanic ash, carbonates and seawater. Below 144.9 mbsf the data plots a straight line, indicating the presence of only two end members, probably pore fluids altered by ash or carbonate diagenesis. The end member with high Sr concentration and radiogenic isotope ratio extrapolates to a value equal to that for the carbonate in the North Aoba Basin sediment. The other end member appears to have both low Sr-isotope ratios and low Sr concentrations. Assuming that the low Sr-isotope ratios result from ash diagenesis, pore fluid with completely exchanged isotopes (i.e., values between 0.703 and 0.704) would have Sr concentrations ranging between 60 and 80 μM (Fig. 13). These concentrations, lower than seawater value, indicate that Sr is lost from the pore fluids during ash diagenesis and the generation of authigenic minerals, for example in the shallow pore fluids where Sr concentrations are less than seawater value (Table 1). Assuming that one of the authigenic clay minerals is smectite, a possible site for this Sr could be substitution for Ca in the smectite.

Accretionary Wedge (Sites 827, 829, 830)

Diagenetic Controls of Solute Concentrations and Isotopic Compositions

At depths less than 100 mbsf at all three accretionary wedge sites the pore fluid composition reflects organic matter diagenesis; SO_4 concentration decreases sharply, while NH_4, PO_4, and alkalinity concentrations increase (Figs. 14, 15, 16). At all three sites, however, the SO_4 concentration increases below the depth of the SO_4 minimum. Because of the extreme care that was taken during handling of the samples the increase in SO_4 concentration is unlikely a result of contamination by the drilling fluid. The deep SO_4-rich pore fluids also contain low Mg concentrations, further indicating there has been little contamination. (Figs. 14, 15, 16). At Sites 827 and 830 the deep SO_4-rich pore fluids were recovered from volcanic breccia units that contain little organic carbon (Fig. 2). Similar to the deep SO_4-rich pore fluids in the North Aoba Basin, this observed increase in SO_4 concentration probably reflects seawater SO_4 trapped during the burial of the organic carbon-poor volcanogenic sediment.

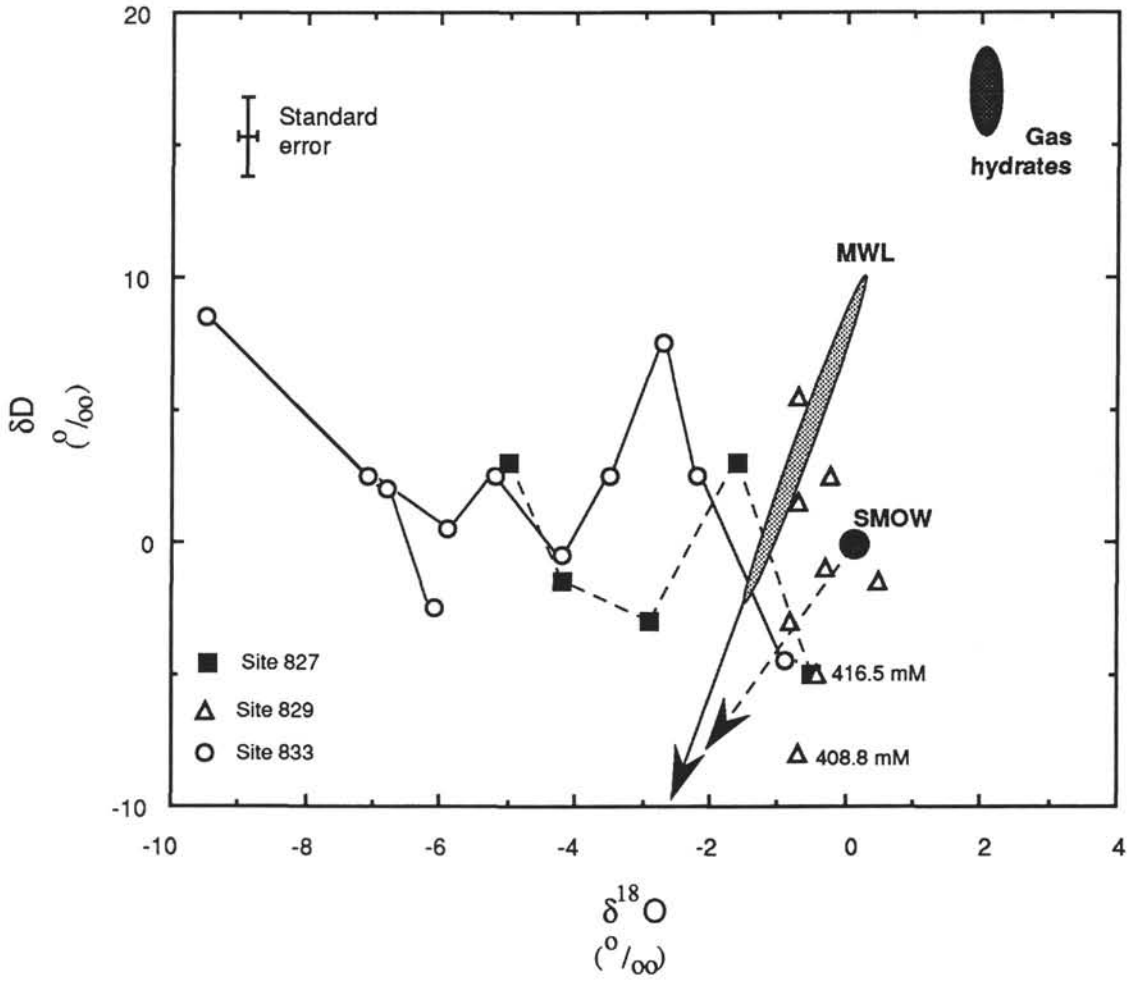

Figure 11. Plot of the pore water $\delta^{18}O$ vs. δD ratios for the North Aoba Basin Site 833 and the accretionary wedge Sites 827 and 829. The solid line with an arrow indicates the meteoric water line (MWL; Craig, 1961), and the dashed line with the arrow indicates the δD-$\delta^{18}O$ correlation (r^2=0.95) for meteoric water from fifteen tropical islands (Dansgaard, 1964). The lightly shaded field on the MWL indicates the expected δD and $\delta^{18}O$ values for low-latitude meteoric water (Dansgaard, 1964). The two low-Cl samples from Site 829 are labeled with their concentrations.

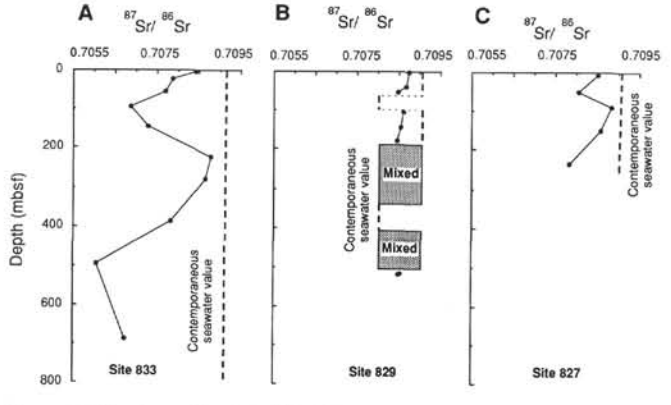

Figure 12. Depth profile of the $^{87}Sr/^{86}Sr$ isotope ratios of the dissolved Sr for **(A)** Site 833, **(B)** Site 829, and **(C)** Site 827. The dashed lines indicate the contemporaneous seawater $^{87}Sr/^{86}Sr$-isotope ratios, and at depths at Site 829 where sediment ages range from Oligocene to Pleistocene due to tectonic mixing the contemporaneous seawater $^{87}Sr/^{86}Sr$ ratios (Elderfield 1986; Hodell et al., 1991) are shown by shaded boxes.

In the accretionary-wedge pore fluid, Cl concentrations are characterized by values both greater and less than seawater value (Fig. 17). At Sites 827 and 830 the concentrations reach maxima of 628 mM and 620 mM, which are intermediate between seawater value and the maxima reached in the North Aoba Basin pore fluids. At Site 829 above 200 mbsf the Cl concentration increases only slightly above seawater value, reaching a maximum concentration of 568 mM. Below 400 mbsf the concentration decreases to a minimum of 409 mM. These are the only pore fluids sampled from the New Hebrides margin with Cl concentrations less than seawater value, an attribute common to convergent margins (Kastner et al., 1991).

At Sites 827 and 830 the major element concentrations show the same exchange of Ca for Na, K, and Mg as the North Aoba Basin pore fluids (Fig. 18). This exchange is best explained by the alteration of volcanic ash to hydrous minerals which could also cause the increased Cl concentrations at these two sites (Fig. 17). At Site 827 the $\delta^{18}O$ values and $^{87}Sr/^{86}Sr$ ratios also indicate large amounts of ash diagenesis (Figs. 9B and 12C). The $\delta^{18}O$ values decrease with depth with approximately the same gradient as at Site 833 (Fig. 9). Although the δD values are scattered at Site 827, most of these pore fluids plot to the left of the meteoric water line, similar to Site 833 (Fig. 11). The $^{87}Sr/^{86}Sr$ ratios show a wide range of values (Table 3), but they are all

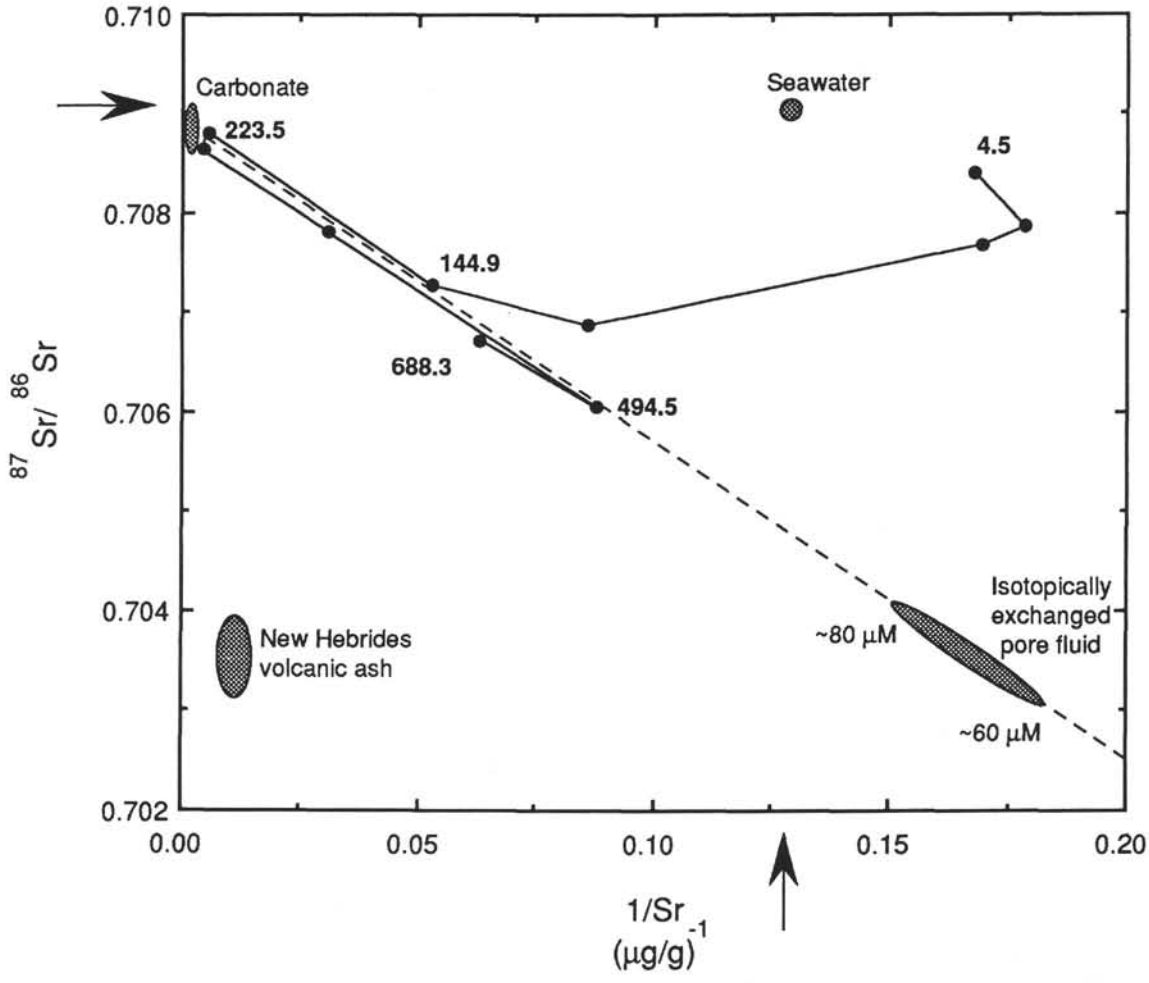

Figure 13. Plot of the $^{87}Sr/^{86}Sr$ isotope ratio vs. 1/Sr concentration of dissolved Sr for the North Aoba Basin Site 833. The 1/Sr concentrations were converted from units of μM^{-1} to $(\mu g/g)^{-1}$, assuming a constant pore-fluid density of 1023 kg/m^3. The isotope ratios and 1/Sr concentrations of possible end-members are shown on the plot, including modern seawater, volcanic ash in the New Hebrides sediments, carbonate minerals, and pore fluid with isotope ratios identical to the New Hebrides ash. The dashed line indicates the linear regression of data from pore fluid at 144.9 mbsf and deeper (n = 6, slope = –0.03215, r^2 = 0.99). Based on this regression line, pore fluid with $^{87}Sr/^{86}Sr$ isotope ratios between 0.704 and 0.703 should have Sr concentrations between 80 and 60 µM. The bold numbers indicate the depths (mbsf) of the samples. The arrows indicate modern seawater value.

lower than the contemporaneous seawater value (Fig. 12C), suggesting isotopic exchange with the ash. The Sr concentrations are somewhat elevated above seawater values (Table 1). If the ash acts as a sink for Sr, as suggested by Figure 13, the elevated Sr concentrations indicate that some Sr was released during carbonate diagenesis, thereby preventing an even greater decrease in the isotope ratios.

Evidence for Fluid Flow

At depths less than 200 mbsf at Site 829 the major element concentrations are less altered from seawater values than at Sites 827 or 830 (Fig. 18), although Sites 827 and 829 are separated by only 1.5 km. Because the geothermal gradient at Site 829 is twice the gradient at Sites 827 and 830 (Fig. 6B), these compositional differences do not result from elevated temperatures increasing the reaction rates at Sites 827 and 830. At these depths the sediments at Site 829 are tectonically mixed by thrusting and consist of Pleistocene ash-rich units and Oligocene to Pleistocene ash-rich carbonate units (Fig. 2). The thrust faults are located at the depths of changes in some of the pore-fluid gradients. The most strongly altered profiles are the Ca, Sr, Li, SO_4, and alkalinity concentrations and the Ca/Mg ratio (Fig. 19), although the NH_4 and PO_4 gradients also exhibit inflections at the same depths (Fig. 15). Although the sharply increasing Ca/Mg ratios could be caused by ash diagenesis in Units I and III, the $\delta^{18}O$ values and Sr isotope ratios indicate only minor ash diagenesis (Figs. 9B and 12B); unlike Site 827, these isotope ratios change only slightly from modern seawater values. The radiogenic $^{87}Sr/^{86}Sr$ ratios and the elevated Sr concentrations indicate that much of the Sr is derived from diagenesis of Tertiary carbonate which also could control the Ca and Ca/Mg profiles (Fig. 19). Because Units I and III are carbonate-poor (Fig. 2), the carbonate diagenesis probably occurs within carbonate-rich Units II and IV through VI.

The higher carbonate content of the Site 829 sediment could be responsible for its different pore-fluid composition from Sites 827 and 830, but these differences could also reflect fluid flow at Site 829 with less, or no, flow at Sites 827 and 830. The small changes in $\delta^{18}O$ values, $^{87}Sr/^{86}Sr$ ratios, and Cl concentrations, even within the ash-rich Units I and III at Site 829, indicate there is less diagenetic alteration to the pore-fluid composition than at Site 827. The altered pore-fluid chemistry at Site 827 could reflect a long residence time and thus little flow and a low water/rock ratio in those sediments. Other indications of more flow at Site 829 than at 827 include porosity

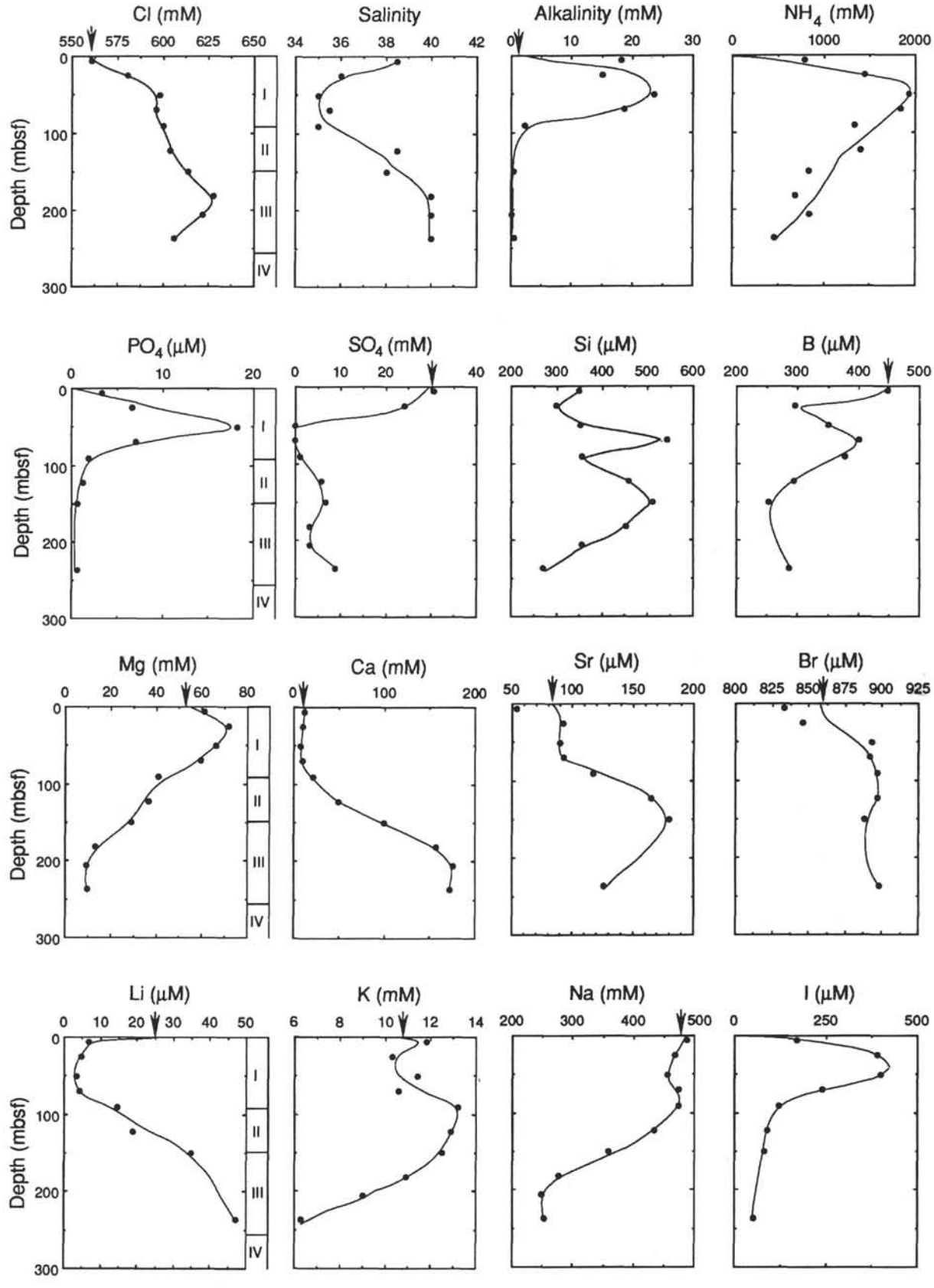

Figure 14. Depth profiles of pore fluid species and unit thicknesses for accretionary wedge Site 827. Arrows indicate seawater composition.

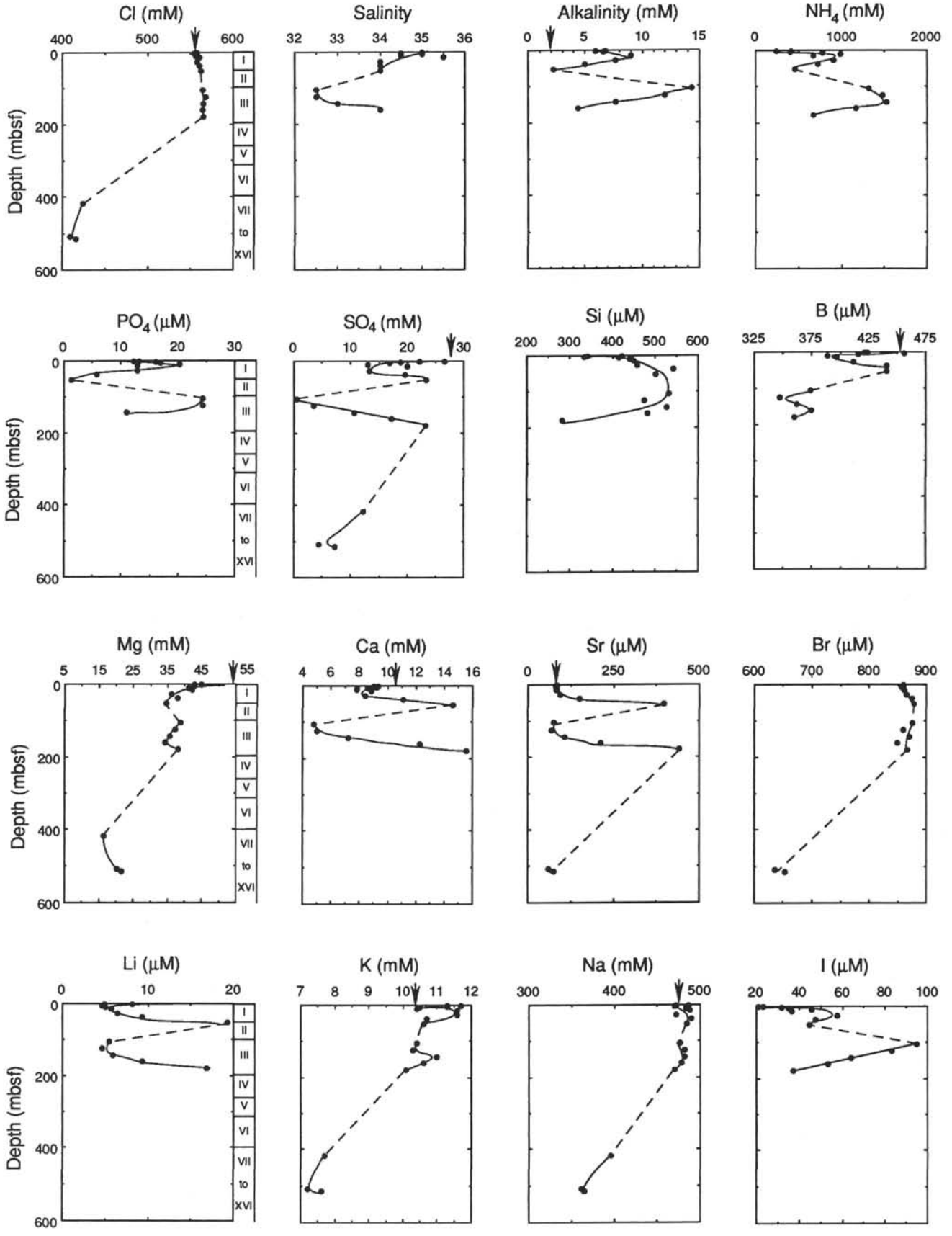

Figure 15. Depth profiles of pore fluid species and unit thicknesses for accretionary wedge Site 829. Because Units VII to XVI are thin (Fig. 2) their boundaries are not marked. Arrows indicate seawater composition.

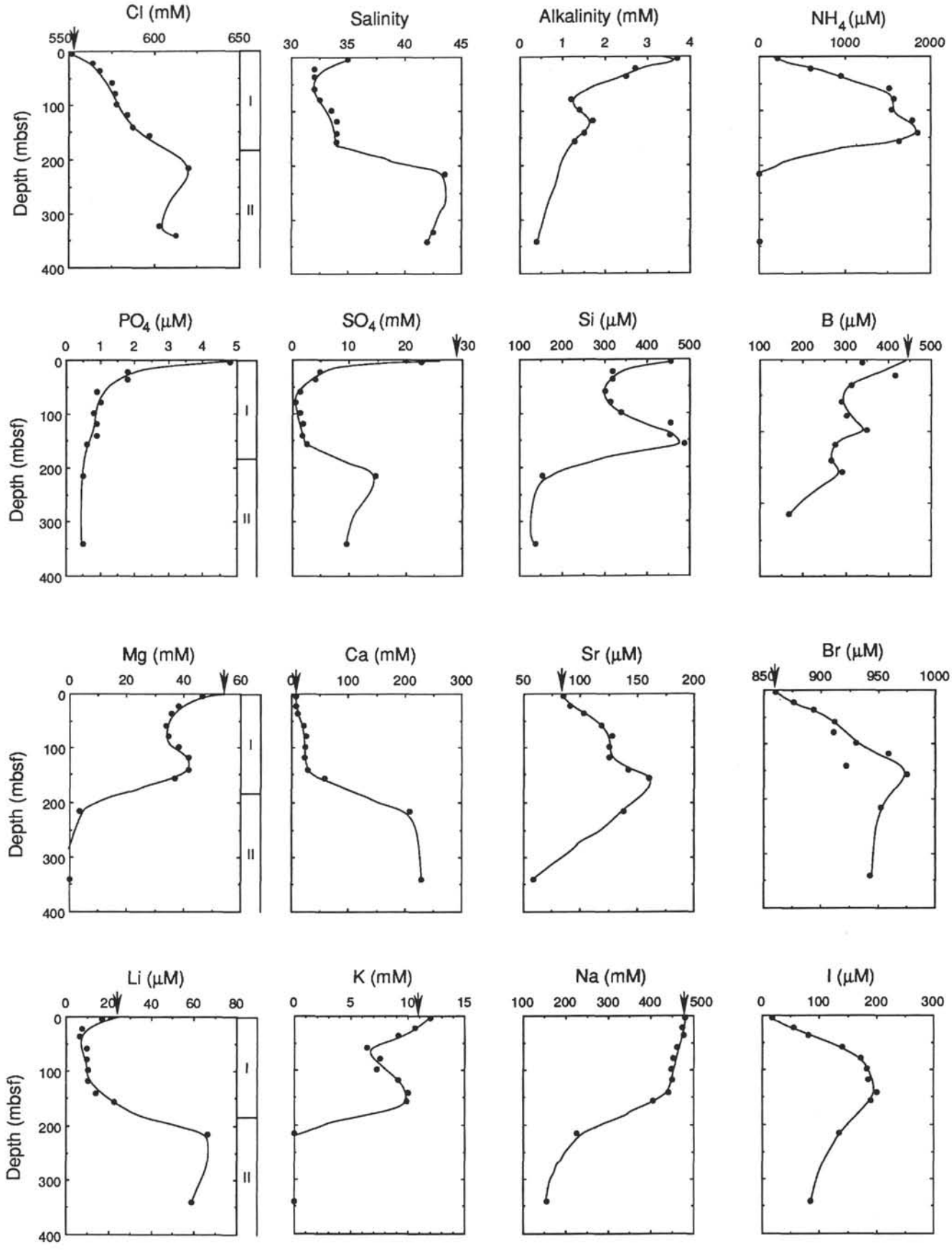

Figure 16. Depth profiles of pore fluid species and unit thicknesses for accretionary wedge Site 830. Arrows indicate seawater composition.

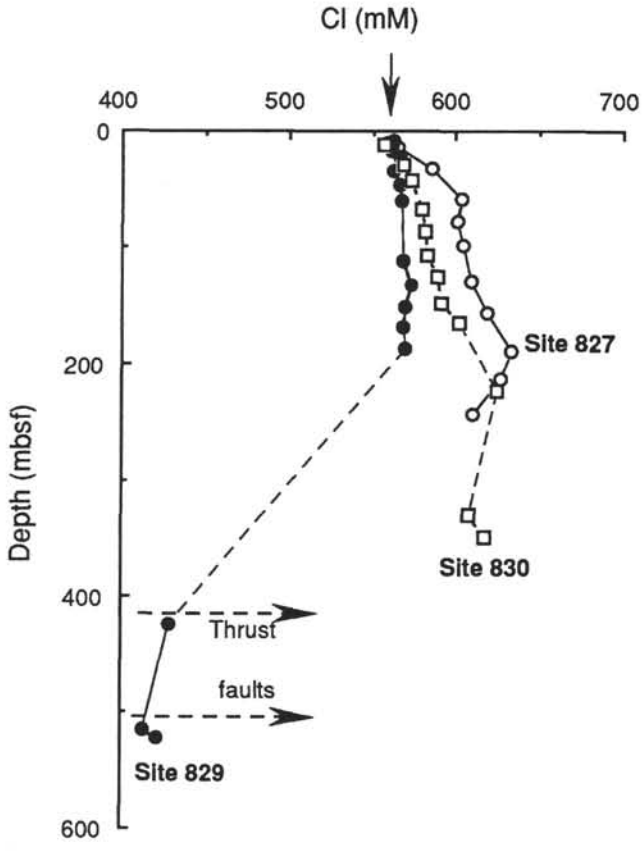

Figure 17. Depth profile of Cl concentrations in the three accretionary wedge Sites 827, 829, and 830. The short horizontal dashed lines with arrows indicate the location of thrust faults at Site 827 (Fig. 2). The arrow indicates seawater value.

and temperature distributions. Modelling indicates that porosity reduction, and thus fluid flow, in accretionary wedges increases from the trench axis toward the volcanic arc (Bekins and Dreiss, 1992). Although Site 829 is closer to the trench than Site 827, porosity reduction is more rapid even within the ash-rich units. The higher temperature gradient at Site 829 than at Sites 827 or 830 could be caused by upward flow of warm water. Likely conduits for flow at Site 829 would be the major thrust faults in the upper 200 m (Fig. 2).

At depths between 200 and 400 mbsf at Site 829, the mixed sediments of Units IV through VI have low porosity (~30%) and water content of approximately 15 to 20% (Leonard and Ask, this volume). The pore-fluid profiles shown in Figure 15 thus lack data between 200 and 400 mbsf. Of the five pristine samples collected and squeezed at depths below 379 mbsf only three yielded fluid (Collot, Greene, Stokking, et al., 1992). These three samples are located less than 20 m below major thrust faults, while the samples yielding no fluid are located less than 25 m above thrust faults. This apparent structural control of the fluid distribution is supported by water content measurements showing two to three times the background water contents in the vicinity of faults. Although some of these elevated water content measurements could be caused by infiltration of drilling fluid, the pore-fluid compositions, discussed in detail below, indicate that some of the fluid is uncontaminated formation fluid.

The deep fluids at Site 829 are characterized by Cl concentrations less than seawater value (Fig. 17), an attribute exhibited by all convergent margins studied (Kastner et al., 1991). Results from a variety of convergent margins (e.g., Blanc et al., 1988, 1991; Gieskes et al., 1990; Kastner et al., 1990; Le Pichon et al., 1990; Gieskes et al., 1993; Mottl et al., 1993) suggest that the low-Cl fluids could originate from several sources. These sources include dilution by a pure water phase released

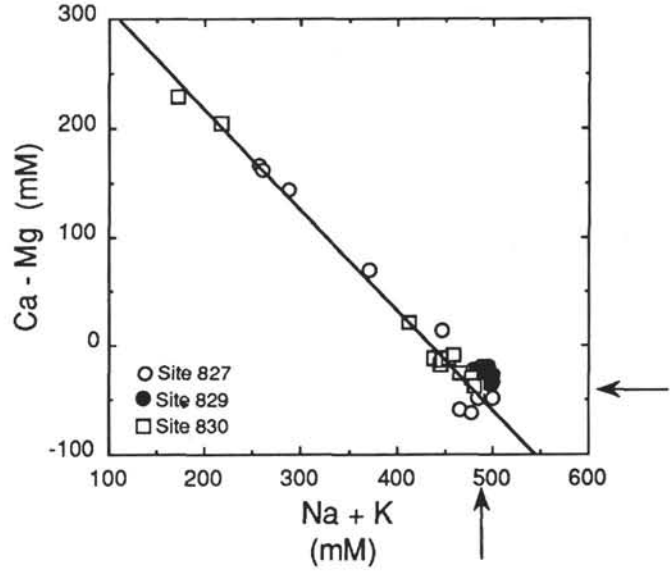

Figure 18. Plot of the Ca minus Mg concentration vs. the Na plus K concentration for the accretionary wedge sites. The arrows indicate seawater values. The solid line indicates a slope of –1

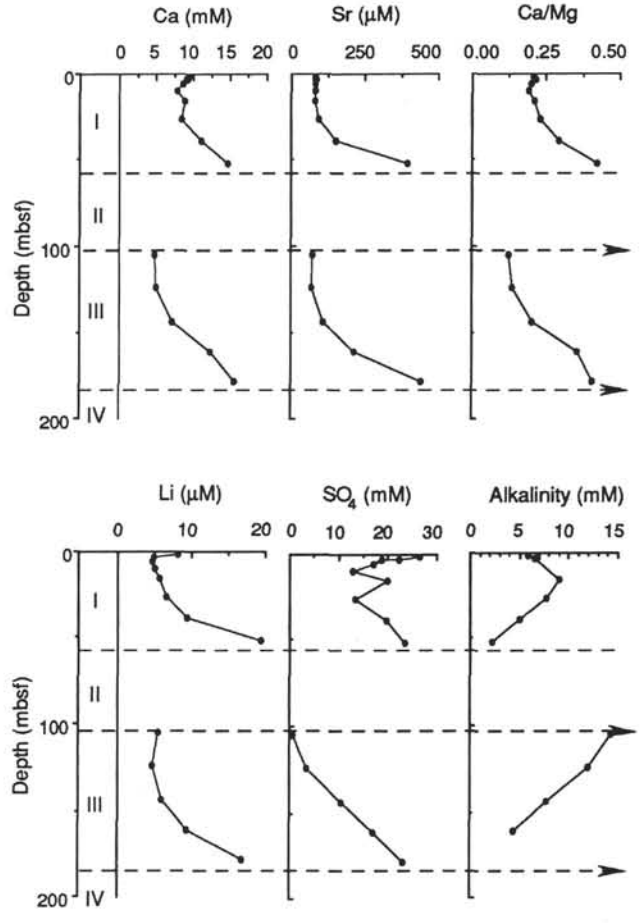

Figure 19. Depth profiles of the Ca, Sr, Li, SO_4, and alkalinity concentrations and the Ca/Mg ratio in the sediments above 200 mbsf at the accretionary wedge Site 829. The boundaries between Units I, II, III, and IV are shown by dashed lines; lines with arrows indicate thrust faults.

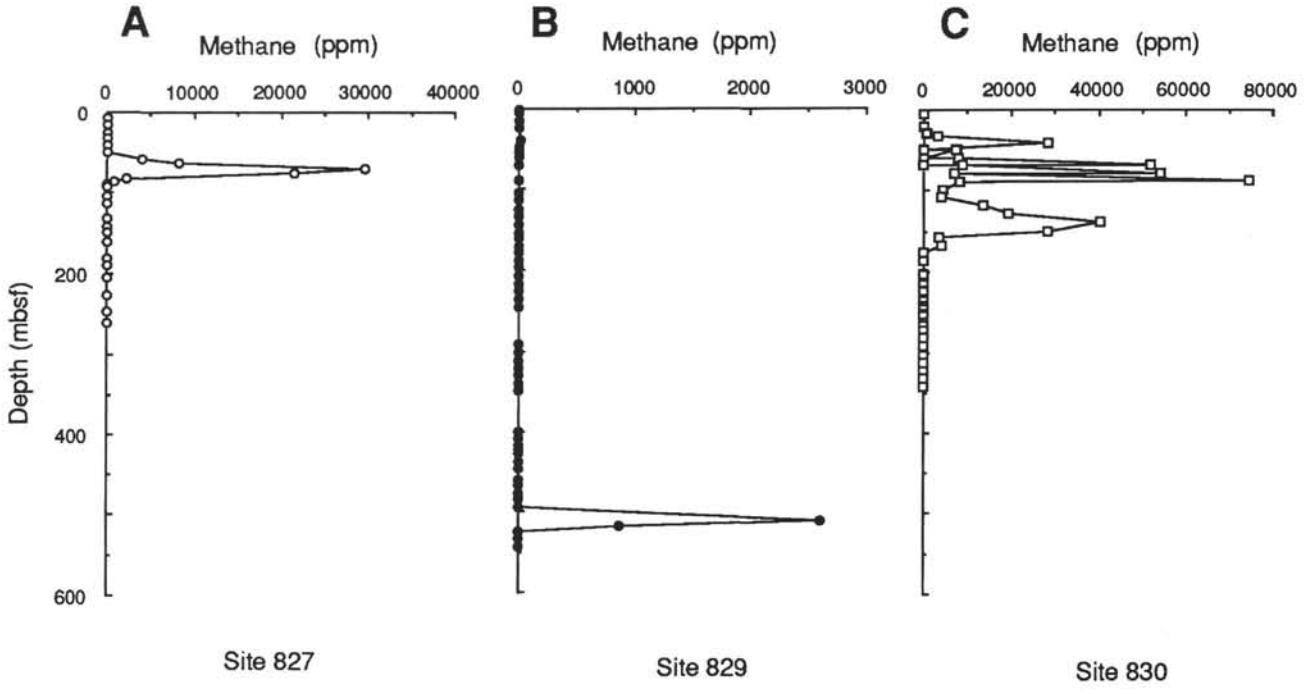

Figure 20. Depth profile of methane concentrations at the accretionary wedge Sites (**A**) 827, (**B**) 829, and (**C**) 830. The units of ppm are on a volume basis (μl/L) and reflect liberation of methane at 70°C from 5 cm^{-3} of sediment into a 21 cm^{-3} vial (Collot, Greene, Stokking, et al., 1992).

during the dissolution of gas hydrates or dehydration of hydrous minerals such as clays and zeolites, dilution by mixing with meteoric water, and also possibly membrane ion filtration (for a description of this process see Kharaka and Berry, 1973; Graf, 1982).

Experimental work shows that during high-pressure filtration, Cl passes more easily through clay membranes than Br, thereby decreasing the Br/Cl ratio in the low-Cl fluid by up to a factor of 10% (Kharaka and Berry, 1973). In the shallow pore fluids at Site 829, the Cl and Br concentrations are near seawater value and thus the Br/Cl ratio is nearly constant at approximately seawater value. The low Cl fluid also has a Br/Cl ratio identical, within error, to seawater ratio, suggesting that membrane filtration is not the cause of the low Cl concentrations (Fig. 8B). The seawater Br/Cl ratio implies that the low Cl concentration results from simple dilution of pore fluids that originally were characterized by seawater Br/Cl ratio.

The dilution is unlikely to have been caused principally by gas hydrate dissociation, although the estimated formation temperatures of about 20°C at the depth of the low Cl fluids are within the stability field of gas hydrates. Assuming a stoichiometry for gas hydrates of $CH_4 \cdot 5.75H_2O$ (Davidson et al., 1978), approximately 2.4 moles of methane per liter of pore water would be liberated in order to produce a sufficient quantity of water to cause the observed 25% decrease in Cl concentrations. For sediments with 20% porosity and assuming that no methane is lost during the core handling and that all the methane is liberated during the head-space procedure, the observed maximum of 2500 ppm methane (Fig. 20B) converts to a concentration of ~0.3 mM methane. Because of the difficulty associated with collecting pristine gas samples, this concentration estimate is probably good only to within an order of magnitude, but it is nearly 4 orders of magnitude less than the amount of methane that would be released from enough gas hydrate to account for the observed dilution. Dense gas hydrate layers appear to be missing from the region because bottom simulating reflectors have not been observed from seismic investigations (Fisher et al., 1991). Gas hydrates are characterized by positive $\delta^{18}O$ and δD values, for example, water from a dissociated gas hydrate collected from the Peru margin had $\delta^{18}O$ and δD values of +1.8‰ and +17.8‰, respectively (Kastner et al., 1990), and $\delta^{18}O$ values up to +2.6‰ of pore water at the Guatemala margin are attributed to gas hydrate dissociation (Hesse and Harrison, 1981). In contrast to these positive values, the low-Cl fluid at Site 829 is characterized by slightly negative $\delta^{18}O$ and δD values (Fig. 11). The low methane concentrations and δD and $\delta^{18}O$ values thus indicate that the dilution does not result only from gas hydrate dissociation.

In order for meteoric water to dilute the Cl concentrations, there must be a source for the water. For example, mixing with meteoric water possibly occurs at the Peru margin (Kastner et al., 1989) and the Barbados accretionary wedge (Le Pichon et al., 1990, 1991), both of which are close to the South American continent. The New Hebrides Island Arc, where only a small area of land is exposed above sea level, is 2000 km from the nearest continent, Australia (Fig. 1), and the island nearest to Site 829, Espiritu Santo, emerged above sea level only 500,000 years ago in conjunction with the collision of the DEZ (Taylor, 1992). A direct conduit from Espiritu Santo Island to Site 829, however, could be provided by several faults that trend perpendicular to the trench axis and which may be connected to onshore faults (Collot and Fisher, 1991). In order for meteoric water to have flowed from Espiritu Santo Island to Site 829, a distance of ~50 km, flow rates on the order of 90 cm/yr would be required.

An additional possible source of low Cl fluids is from the dehydration of clay and zeolite minerals. The observed 25% decrease in Cl concentration from seawater value (Fig. 17) requires approximately 0.05 m^3 water/m^3 sediment for sediment with ~20% porosity such as at Site 829. Kastner et al. (1991) calculated that complete dehydration of sediment containing 20 wt% smectite and 30% porosity would provide 0.021 m^3 water/m^3 sediment. Higher clay contents, breakdown of clay minerals and the release of structural water and dehydration of the oceanic crust would provide additional water. Sufficient water for the observed dilution at Site 829 thus could be produced through mineral dehydration alone.

The $\delta^{18}O$ and δD values indicate several sources may contribute to the low-Cl fluid. The $\delta^{18}O$ value of water released from hydrous minerals should be positive, but the observed $\delta^{18}O$ values of the low-Cl fluids are negative, with values of –0.7% and –0.4‰ (Table 2). These values are heavier relative to their δD values than those

expected from meteoric water at low latitudes and on tropical islands (Fig. 11). The isotope ratios therefore suggest that the source of the fluid is a mixture of meteoric water and water released during mineral dehydration. Because precise isotopic values of the possible mineral and meteoric water sources are unknown, the relative proportions from each source cannot be evaluated.

Based on the temperature gradient shown in Figure 6B, temperatures of ~20°C at 400 to 500 mbsf are ~40°C lower than those required for dehydration of interstitial or channel water (Colton-Bradley, 1987). Such temperatures will occur at >1.5 km burial depth at Site 829 and even greater depths for Site 827 and 830 because of their lower temperature gradients. Advection of the deep fluid is required in order for water released below 1.5 km to dilute the fluids at 400 mbsf; elevated water contents near fault zones suggest that advection occurs along the fault planes. Advection along faults of low-Cl water has previously been proposed to explain low-Cl and methane-rich fluid found in the Barbados accretionary wedge (Blanc et al., 1988, 1991; Gieskes et al., 1990; Vrolijk et al., 1990, 1991). The methane in the Barbados water has been identified as thermogenic based on its isotope ratio and the presence of heavier hydrocarbons supporting a deep origin of the fluids. In the New Hebrides margin, the low-Cl fluid also contains methane (Fig. 20). No heavier hydrocarbons were observed and the isotope ratios of this gas have not been measured, and thus the gas origin, whether biogenic or thermogenic, is unknown.

CONCLUSIONS

Results from the New Hebrides margin show that fluid with seawater composition can be extensively and rapidly altered into a $CaCl_2$ brine simply through exchange reactions with the solid phases and authigenesis of hydrous minerals. Assuming that the North Aoba Basin brines are formed in situ and have not flowed from elsewhere, at a maximum they should be of the same age as the surrounding sediments. These maximum ages are only between 0.45 and 1.89 Ma at the burial depths of volcanic breccias at Sites 832 and 833. Minor element concentrations are also altered by this diagenesis. For example, Sr appears to be incorporated into authigenic silicate minerals. In contrast with Sr, however, Li appears to be only initially incorporated into the solid phases; subsequently, at greater burial depths it seems to be released. This change in behavior could be due to temperature-dependent reactions, as observed experimentally by Seyfried et al. (1984), which shows that Li is removed from pore fluids and incorporated into solids at temperatures <150°C. Results from the New Hebrides margin suggest that Li may be leached from solid phases at temperatures less than experiments indicate: Li maxima occur at depths of only 300 mbsf where temperatures are probably <35°C.

The New Hebrides margin also provides additional information about the hydrologic behavior of fluids at convergent margins. Fluid flow and the lack of flow appear to affect the extent of chemical and isotopic alteration of the accretionary wedge pore fluid. Fluid flow seems to be fault controlled, and those regions with few or no faults appear to have little or no flow. Because regions with no flow are subjected to the same tectonic stresses as regions with flow, pore pressures must increase in the absence of fluid flow. Much of the fluid flowing in the shallow sediments appears to be forced through the sediment during porosity reduction with little, or no, additional fluid from external sources. The low-Cl concentration of some fluid at greater depths results from mixing between meteoric water, water released from clay and mineral dehydration and the original pore fluids. Methane concentrations suggest that only minor water would be released from gas-hydrate dissociation, and the Br/Cl ratio indicates that membrane filtration is unimportant.

The New Hebrides sediment is composed of fractions of hydrous minerals larger than those of most other studied margins. Based on the Cl dilution, this source will provide only ~0.05 m^3 H_2O/m^3 sediments and even less if some of the dilution results from meteoric water mixing. Results from deep submersible dives (Greene et al., 1992) indicate that surface manifestations of fluid venting (e.g., sulfide-oxidizing benthic biota, carbonate crusts, and mud volcanoes) are sparse or missing completely from the margin, implying that there is a smaller fluid flux than from other previously studied margins. This apparently smaller flux could be caused by minimal recharge of meteoric water because of the short time of exposure of land in the region and small geographic exposure of the land. Other water sources, such as gas hydrate dissociation, also appear to be missing from the margin.

ACKNOWLEDGMENTS

I am grateful for the superb assistance provided by the crew and technical staff aboard the *JOIDES Resolution*, especially the two Leg 134 chemistry technicians, MaryAnn Cusimano and Mark Simpson, who not only helped with the analyses, but also made the cruise more pleasant. I thank the co-chief scientists, Jean-Yves Collot and Gary Greene for allowing me to take many extra, and occasionally extraordinarily long, samples that were extremely valuable for this paper. I also thank Gunter Lugmair and Doug Macdougall for the use of their laboratory for the Sr isotope measurements and Ellen Martin for her patience in teaching me the Sr isotope techniques, and for her support in general. The paper has been improved by numerous thoughtful suggestions by Steve Chambers, Joris Gieskes, and Miriam Kastner and careful and conscientious reviews by Gerard Blanc, Jean-Yves Collot, and an anonymous reviewer. This work was supported by a JOI-United States Science Advisory Committee (USSAC) grant.

REFERENCES*

Bekins, B.A., and Dreiss, S.J., 1992. A simplified analysis of parameters controlling dewatering in accretionary prisms. *Earth Planet Sci. Lett.*, 109:275–287.

Blanc, G., Boulegue, J., and Gieskes, J.R., 1991. Chemical evidence for advection of interstitial fluid in the sedimentary series of the Barbados accretionary complex (Leg 110). *Oceanol. Acta*, 14:33–49.

Blanc, G., Gieskes, J.M., Vrolijk, P.J., et al., 1988. Advection de fluides interstitiels dans les séries sédimentaires du complexe d'accrétion de la Barbade (Leg 110 ODP). *Bull. Soc. Geol. Fr.*, 8:453–460.

Blanc, G., Hawkins, J., Parson, L.M., Allan, J., et al., 1991. ODP Leg 135 Pacifique: Bassin de Lau. *Geochronique*, 40:9.

Bray, C.J., and Karig, D.E., 1985. Porosity of sediments in accretionary prisms, and some implications for dewatering processes. *J. Geophys. Res.*, 90:768-778.

Carson, B., Suess, E., and Strasser, J.C., 1990. Fluid flow and mass flux determinations at vent sites on the Cascadia margin accretionary prism. *J. Geophys. Res.*, 95:8891–8898.

Chambers, S.R., and Cranston, R.E., 1991. Interstitial-water geochemistry of Kerguelen Plateau sediments. *In* Barron, J., Larsen, B., et al., *Proc. ODP, Sci. Results*, 119: College Station, TX (Ocean Drilling Program), 347–374.

Collot, J.-Y., Daniel, J., and Burne, R.V., 1985. Recent tectonics associated with the subduction/collision of the d'Entrecasteaux zone in the central New Hebrides. *Tectonophysics*, 112:325–356.

Collot, J.-Y., and Fisher, M.A., 1991. The collision zone between the North d'Entrecasteaux Ridge and the New Hebrides Island Arc. Part 1: Seabeam morphology and shallow structure. *J. Geophys. Res.*, 96:4457–4478.

Collot, J.-Y., Greene, H.G., Stokking, L.B., et al., 1991. *Proc. ODP, Init. Repts.*, 134: College Station, TX (Ocean Drilling Program).

Colten-Bradley, V.A., 1987. Role of pressure in smectite dehydration—effects on geopressure and smectite-to-illite transformation. *AAPG Bull.*, 71: 1414–1427.

COSOD II, 1987. *Rep. 2nd Conf. Sci. Ocean Drilling*, Strasbourg, France, (European Science Foundation).

Craig, H., 1961. Isotopic variations in meteoric waters. *Science*, 133:1702-1703.

Daniel, J., and Katz, H.R., 1981. d'Entrecasteaux zone, trench and western chain of the central New Hebrides Island Arc: their significance and tectonic relationship. *Geo-Mar. Lett.*, 1:213–219.

* Abbreviations for names of organizations and publications in ODP reference lists follow the style given in *Chemical Abstracts Service Source Index* (published by American Chemical Society).

Dansgaard, W., 1964. Stable isotopes in precipitation. *Tellus,* 16:436–468.
Davidson, D.W., El-Defrawy, M.K., Fuglen, M.D., and Judge, A.S., 1978. Natural gas hydrates in northern Canada. *Proc. 3rd Int. Conf. on Permafrost,* 3:937–943.
Egeberg, P.K., and Leg 126 Shipboard Scientific Party, 1990. Unusual composition of pore-waters found in the Izu-Bonin fore-arc sedimentary basin. *Nature,* 344:215–218.
Elderfield, H., 1986. Strontium isotope stratigraphy. *Palaeogeogr., Palaeoclimatol., Palaeoecol.,* 57:71–90.
Faure, G., 1986. *Principles of Isotope Geology*: New York (Wiley).
Fisher, M.A., Collot, J.-Y., and Geist, E.L., 1991. The collision zone between the North d'Entrecasteaux Ridge and the New Hebrides Island Arc. Part 2: structure from multichannel seismic data. *J. Geophys. Res.,* 96:4479–4495.
Fowler, S.R., White, R.S., and Louden, K.E., 1985. Sediment dewatering in the Makran accretionary prism. *Earth Planet. Sci. Lett.,* 75:427–438.
Gieskes, J.M., 1981. Deep-sea drilling interstitial water studies: implications for chemical alteration of the oceanic crust, layers I and II. *In* Warme, J.E., Douglas, R.G., and Winterer, E.L. (Eds.), *The Deep Sea Drilling Project: A Decade of Progress.* Spec. Publ.—Soc. Econ. Paleontol. Mineral., 32:149–167.
Gieskes, J.M., Gamo, T., and Brumsack, H.J., 1991. Chemical methods for interstitial water analysis aboard *JOIDES Resolution. ODP Tech. Note,* 15.
Gieskes, J.M., Gamo, T., and Kastner, M., 1993. Major and minor element geochemistry of interstitial waters of Site 808, Nankai trough: an overview. *In* Hill, I.A., Taira, A., Firth, J.V., et al., *Proc. ODP, Sci. Results,* 131: College Station, TX (Ocean Drilling Program).
Gieskes, J.M., Vrolijk, P., and Blanc, G., 1990. Hydrogeochemistry, ODP Leg 110: an overview. *In* Moore, J.C., Mascle, A., et al., *Proc. ODP, Sci. Results,* 110: College Station, TX (Ocean Drilling Program), 395–408.
Gill, J.B., 1981. *Orogenic Andesites and Plate Tectonics*: New York (Springer-Verlag).
Graf, D.L., 1982. Chemical osmosis, reverse chemical osmosis, and the origin of subsurface brines. *Geochim. Cosmochim. Acta,* 46:1431–1448.
Greene, H.G., Collot, J.-Y., Pelletier, B., and Lallemand, S., 1992. Observation of forearc seafloor deformation along the north D'Entrecasteaux Ridge-New Hebrides Island Arc collision zone from *Nautile* submersible. *In* Collot, J.-Y., Greene, H.G., Stokking, L.B., et al., *Proc. ODP, Init. Repts.,* 134: College Station, TX (Ocean Drilling Program), 43–53.
Greene, H.G., and Wong, F.L. (Eds.), 1988. *Geology and Offshore Resources of Pacific Island Arcs—Vanuatu Region.* Circum-Pac. Counc. Energy and Miner. Resour., Earth Sci. Ser., 8.
Han, M.W., and Suess, E., 1989. Subduction induced pore fluid venting and the formation of authigenic carbonates along the Cascadia continental margin: implications for the global Ca-cycle. *Palaeogeogr., Palaeoclimatol., Palaeoecol.,* 71:97–118.
Hesse, R., and Harrison, W.E., 1981. Gas hydrates (clathrates) causing pore water freshening and oxygen isotope fractionation in deep-water sedimentary sections of terrigenous continental margins. *Earth Planet. Sci. Lett.,* 55:453–462.
Hodell, D.A., Mueller, P.A., and Garrido, J.R., 1991. Variations in the strontium isotopic composition of seawater during the Neogene. *Geology,* 19:24–27.
Holser, W.T., 1966. Bromide geochemistry of salt rocks. *In* Rau, J.L. (Ed.), *Proc. 2nd Symp. on Salt.* Ohio Geol. Soc., 248–275.
————, 1970. Bromide geochemistry of some non-marine salt deposits in the southern Great Basin. *Mineral. Soc. Am., Spec. Pap.,* 3:307–319.
————, 1979. Trace element and isotopes in evaporites. *Mineral. Soc. Am. Rev.,* 6:295–346.
Holser, W.T., and Wilgus, C.W., 1981. Bromide profiles of the Röt salt, Triassic of northern Europe as evidence of its marine origin. *Neues Jahrb. Mineral. Mb.,* 6:267–276.
Kastner, M., Elderfield, H., and Martin, J.B., 1991. Fluids in convergent margins: what do we know about their composition, origin, role in diagenesis and importance for oceanic chemical fluxes? *Philos. Trans. R. Soc. London A,* 325:243–259.
Kastner, M., Elderfield, H., Martin, J.B., Suess, E., Kvenvolden, K.A., and Garrison, R.E., 1990. Diagenesis and interstitial-water chemistry at the Peruvian continental margin—major constituents and strontium isotopes. *In* Suess, E., von Huene, R., et al., *Proc. ODP, Sci. Results,* 112: College Station, TX (Ocean Drilling Program), 413–440.
Kastner, M., Martin, J.B., and Elderfield, H., 1989. The source of low chloride fluids in the upper slope of the Peruvian continental margin. *In Epstein's 70th Birthday Symp.* California Inst. Technol., 1–2.
Kharaka, Y.K., and Berry, F.A., 1973. Simultaneous flow of water and solute through geological membranes. I: experimental investigations. *Geochim. Cosmochim. Acta,* 37:2577–2603.
Lancelot, Y., Larson, R., et al., 1990. *Proc. ODP, Init. Repts.,* 129: College Station, TX (Ocean Drilling Program).
Lawrence, J.R., and Gieskes, J.M., 1981. Constraints on water transport and alteration in the oceanic crust from the isotopic composition of pore water. *J. Geophys. Res.,* 86:7924–7934.
Lawrence, J.R., Gieskes, J.M., and Broecker, W.S., 1975. Oxygen isotope and cation composition of DSDP pore water and the alteration of layer II basalts. *Earth Planet. Sci. Lett.,* 27:1–10.
Le Pichon, X., Foucher, J.-P., Boulegue, J., Henry, P., Lallemant, S., Benedetti, M., Avedik, F., and Mariotti, A., 1990. Mud volcano field seaward of the Barbados accretionary complex: a submersible survey. *J. Geophys. Res.,* 95:8931–8943.
LePichon, X., Henry, P., and the Kaiko Scientific Crew, 1991. Water budgets in accretionary wedges: a comparison. *Philos. Trans. R. Soc. London A,* 335:315–330.
Marthelot, J.-M., Chatelain, J.L., Isacks, B.L., Cardwell, R.K., and Coudert, E., 1985. Seismicity and attenuation in the central Vanuatu (New Hebrides) islands: a new interpretation of the effect of subduction of the d'Entrecasteaux fracture zone. *J. Geophys. Res.,* 90:8641–8650.
Martin, J.B., Kastner, M., and Elderfield, H., 1991. Lithium: sources in pore fluids of Peru slope sediments and implications for oceanic fluxes. *Mar. Geol.,* 102:281–292.
McDuff, R.E., and Gieskes, J.M., 1976. Calcium and magnesium profiles in DSDP interstitial waters: diffusion or reaction? *Earth Planet. Sci. Lett.,* 33:1–10.
Moore, J.C., Mascle, A., Taylor, E., Alvarez, F., Andreieff, P., Barnes, R., Beck, C., Behrmann, J., Blanc, G., Brown, K., Clark, M., Dolan, J., Fisher, A., Gieskes, J., Hounslow, M., McClellan, P., Moran, K., Ogawa, Y., Sakai, T., Schoonmaker, J., Vrolijk, P.J., Wilkens, R., and Williams, C., 1987. Expulsion of fluids from depth along a subduction-zone decollement horizon. *Nature,* 326:785–788.
Mottl, M.J., 1992. Pore waters from serpentinite seamounts in the Mariana and Izu-Bonin forearcs, Leg 125: evidence for volatiles from the subducting slab. *In* Fryer, P., Pearce, J.A., Stokking, L.B., et al., *Proc. ODP, Sci. Results,* 125: College Station, TX (Ocean Drilling Program), 373–385.
Newman, A.C.D. (Ed.), 1987. *Chemistry of Clays and Clay Minerals:* New York (Wiley), Mineral. Soc. London Monogr., 6.
Parson, L., Hawkins, J., Allan, J., et al., 1992. *Proc. ODP, Init. Repts.,* 135: College Station, TX (Ocean Drilling Program).
Robie, R.A., Hemingway, B.S., and Fisher, J.R., 1979. *Thermodynamic Properties of Minerals and Related Substances at 298.15 K and 1 bar (10^5* Pascals) Pressure and at Higher Temperatures. U.S. Geol. Surv. Bull., 1452.
Sand, L.B., and Mumpton, F.A. (Eds.), 1978. *Natural Zeolites: Occurrence, Properties, Use:* New York (Pergamon Press).
Savin, S.M., 1967. Oxygen and hydrogen isotope ratios in sedimentary rocks and minerals [Ph.D. dissert.]. California Inst. of Technol.
Seyfried, W.E., Janecky, D.R., and Mottl, M.J., 1984. Alteration of oceanic crust: implications for geochemical cycles of lithium and boron. *Geochim Cosmochim. Acta,* 48:557–569.
Taylor, F.W., 1992. Quaternary vertical tectonics of the central New Hebrides Island Arc. *In* Collot, J.-Y., Greene, H.G., Stokking, L.B., et al., *Proc. ODP, Init. Repts.,* 134: College Station, TX (Ocean Drilling Program), 33–42.
von Huene, R., and Lee, H.J., 1983. The possible significance of pore fluid pressures in subduction zones. *In* Watkins, J.S., and Drake, C.L. (Eds.), *Studies in Continental Margin Geology.* AAPG Mem., 34:781–789.
Vrolijk, P., Chambers, S.R., Gieskes, J.M., and O'Neil, J.R., 1990. Stable isotope ratios of interstitial fluids from the Northern Barbados Accretionary Prism, ODP Leg 110. *In* Moore, J.C., Mascle, A., et al., *Proc. ODP, Sci. Results,* 110: College Station, TX (Ocean Drilling Program), 189–205.
Vrolijk, P., Fisher, A., and Gieskes, J., 1991. Geochemical and geothermal evidence for fluid migration in the Barbados accretionary prism (ODP Leg 110). *Geophys. Res. Lett.,* 18:947–950.

Date of initial receipt: 16 April 1992
Date of acceptance: 30 October 1992
Ms 134S-008